Ground magnetic profiling of faults in the Albuquerque Basin, NM: Implications for fault structure in sedimentary basins

Brant W. Cole
Earth and Environmental Science Department
New Mexico Institute of Mining and Technology
Socorro, NM 87801

An independent study submitted in partial fulfillment of the requirements for the Degree, Master of Science in Geophysics from the Department and Environmental Science, New Mexico Institute of Mining and Technology.

2003

Table of Contents

Heading	Page
I. Introduction	1
II. Magnetics Theory	4
III. Geological Setting	8
IV. Methods	12
Equipment	
Procedure	
Data	
V. Qualitative discussion on anomalies/data	26
Continuation Effects	
Aeromagnetic versus ground data comparison	
Anomaly pattern discussion	
Anomaly spatial relation	
Qualitative analysis	
Topographic effects	
VI. Model results and discussion	36
Topography	
Simple Models	
Furthering models	
SHF1	
SHF2	
SHF3	

SHF4

SHF5

SHF6

SHF7

Spatial relationships of models

Conclusions 65

Appendix A 67

References 69

I. Introduction

Faults in sedimentary basins have long been a source of interest, though not well understood. Poorly consolidated sediments intermixed with low permeability clays and numerous faults can act as traps for hydrocarbon emplacement, as well as various aquifers that are used as sources of water (Heynekamp, 1998; Anderson et al., 1998). In the Albuquerque Basin, where water rights and recharge/discharge of water are extremely important issues, fault structure is imperative to know and understand. Faults can act either as preferential fluid flow mechanisms or impermeable barriers. The ability to map these faults gives additional insight into the delineation of relative size and shape of hydrostratigraphic units (Grauch, 2001; Hawley et al., 1992).

Many of the standard means of fault locating are imprecise or unsuitable for analysis in sedimentary basins. Many faults go undetected by surface fault mapping, especially smaller scale faults that do not contain enough displacement to make noticeable contrasts through loose sediments. Faults mapped in the basement by typical seismic procedures cannot always be traced up through the sedimentary section to show the extent of faulting. Seismic investigation may also be extremely expensive to employ, and suffers when there is a lack of strong contrasts of physical properties in fault areas located within sedimentary fill. Drilling a large number of wells for exploration purposes is also not feasible due to the expense of drilling and time factors involved in constraining the properties of an entire basin. A method to quickly and inexpensively determine fault relation/orientation in sedimentary basins is necessary, as the question of how fault structure and related structures affect groundwater flow is key to the

understanding of current water flow properties and planning for future water uses and land rights issues.

Magnetic methods are widely used and have the most widespread coverage in terms of square miles of any geophysical method/instrument to date. This is due to magnetic methods being both cost effective and readily producing data for three-dimensional maps that can be easily related to geological and other information (Redford, 1980). Magnetics, primarily aeromagnetics, has long been used in applications primarily associated with deep basement rock mapping, assuming magnetically transparent sedimentary sections overlain on the basement rocks (Gibson and Millegan, 1998). As instrument precision and processing techniques have been improved, smaller localized features have begun to be interpreted (Gibson and Millegan, 1998). The advances of magnetics as an investigative technique from the 1930's to 1980's are well covered in Redford (1980) and Paterson (1985). Increased resolution surveys and details of more recent studies can be found in Gibson and Millegan (1998) and Society of Exploration Geophysicists (1998 and 2001). These features include near-surface fault mapping in sedimentary basins, which can be used to answer and facilitate understanding of a variety of scenarios pertaining to sedimentary basin structure.

In 1996 and 1997, the United States Geologic Survey (USGS), as part of the Middle Rio Grande Basin Study, contracted a series of high-resolution aeromagnetic surveys for investigation of faulted areas within the Albuquerque Basin (Grauch et al., 2001). The data collected show a series of complex linear features that were interpreted

as faults. As the aeromagnetic data was compared to mapped faults and showed a generally strong correlation of anomalies associated with mapped fault structures, the question arose of the subsurface cause of the anomalies. Grauch et al. (2001) concluded that the juxtaposition of syntectonic depositional layers with differing magnetic properties in the upper 500 meters of the subsurface is the cause of these anomalies. This idea of syntectonic depositional magnetization was a departure from the previous ideas of magnetization being localized along the fault plane via geochemical alteration related to fluid flow as the source for fault anomalies in magnetics data (Peirce, 1998), biological alteration, and/or primary basement juxtaposition within these poorly consolidated basins.

The study that is the focus of this paper came about from the desire to understand how the magnetic parameters and the structure are related within the fault complex in more depth. Ground magnetic profiles were used to study features in the subsurface at smaller scale. The Sand Hill Fault was chosen based on the large amount of studies on this fault and the reasonably good constraints on the geological structure. This fault zone displays some of the more prominent and complex aeromagnetic signatures related to fault structures. Several important questions stem from this complex relationship of the aeromagnetic signature to the fault structures. First, are the anomalies just a feature of topography and what is the overall relation of topography to the magnetic anomalies? Second, what causes certain anomalies to be offset towards the west from the mapped fault? Thirdly, what is the cause of areas where the Sand Hill fault has been mapped, but no aeromagnetic anomaly is found? The main question through the entirety of this

investigation is, what is the relation of the known geology of the Sand Hill Fault and the magnetic anomalies and associated models of both the ground survey and the USGS aeromagnetic survey?

II. Magnetics Theory

The interaction of the Earth's natural magnetic field and materials located within the subsurface capable of being magnetized is the basis for this type of research. The Earth's magnetic field is commonly modeled as a dipole magnet located through the center of the Earth that is slightly inclined (Figure 1)(Lillie, 1999). This dipole is situated approximately 11.5° from the earth's axis of rotation, with corresponding north and south polls. As with a bar magnet, the Earth's magnetic field strength is highest at it poles (~60,000nT) and weakest at the equator (~30,000nT) (Figure 1)(Lillie, 1999). This dipole model is only good to a first approximation; as in actuality the Earth's magnetic field requires numerous smaller dipoles to complement the main one in order to completely model the true magnetic field (Sharma, 1976).

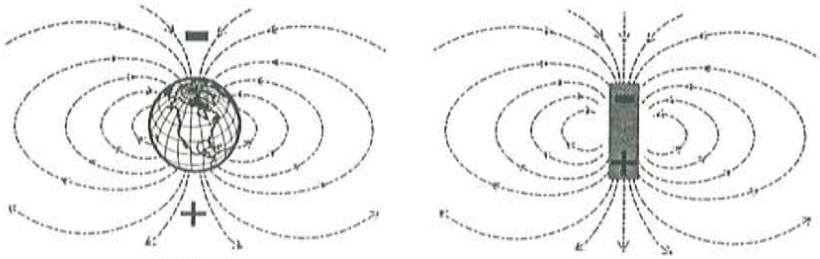

Figure 1. Picture showing the a) Earth's magnetic field and relation to b) a bar magnet. Taken from Lillie (1999)

There are three main components to the Earth's magnetic field that are used to define it: intensity, inclination, and declination. The total field strength, or intensity, is the value of the magnetic field considered at a point of the surface. The magnetic inclination is the angle that the magnetic field lines, which emanate from all points on the Earth's surface, make with the horizontal ground surface (0° at the equator and 90° at the poles) (Reynolds, 1997). The magnetic declination is the angle the magnetic field lines make with geographic north. All three components, intensity, inclination, and declination, depend on the latitude at a particular location on the Earth (Reynolds, 1997). Standard tables of inclination, declination, and field strength are regularly produced as in the International Geomagnetic Reference Field (IGRF) (Reynolds, 1997).

As the Earth's magnetic field is well defined with constrained inclinations, declinations, and intensity along the entire Earth's surface, a magnetics survey attempts to detect small-scale variations from the expected field. These variations are a product of magnetized objects within the subsurface of the Earth. The magnetization of these objects is either induced or remanent.

Induced magnetization is the interaction of the Earth's total magnetic field with the susceptibility of a rock. Magnetic susceptibility is an inherent property of all rock materials; it is the ability of a material to become magnetized. A material that has a small positive susceptibility will induce a small, secondary magnetic field in the presence of the main magnetic field. These induced magnetic fields in the subsurface cause the variations that are measured, generally referred to as anomalies (Reynolds, 1997). These

anomalies locally affect both the direction and magnitude of the Earth's magnetic field when measurements are taken near that specific area. These anomalies are used to interpret what is in the subsurface structure (Reynolds, 1997).

Remnant magnetization is the second magnetic property of rocks with susceptibilities. In this process rocks retain an induced field, which stays permanently with the rock. It is dependent upon magnetic materials getting locked into place, either via quickly cooling volcanic deposition or diagenetic processes (Reynolds, 1997). This becomes important in instances where the remnant magnetization is on the same order of magnitude or much greater than the induced magnetization. In these instances, the remnant magnetization can overprint the induced signal and give erroneous interpretations, unless considered in the modeling applications (Reynolds, 1997). In this study, the remnant magnetization is considered negligible. A previous survey of the relation of remnant to induced magnetization in the Albuquerque Basin found Koenigsberger ratios of 0.4 to 0.6 (Grauch et al., 2001; Hudson et al., 1999). Koenigsberger ratios are simply the ratio of remanent magnetization to induced magnetization. These are sufficiently low enough (under 1) to allow the effect of remnant magnetization to be ignored in this study.

Localized Magnetic Theory

Minerals are classified based on their magnetic susceptibilities, as either diamagnetic or paramagnetic. Diamagnetic minerals have small negative susceptibilities, but these values are very low and do not have an effect in an exploration survey (Burger,

1992). Paramagnetic minerals have small positive susceptibilities in general, but in a few cases atomic orbital motions and electron interactions can produce a strong magnetic effect (Burger, 1992). These strong paramagnetic mineral susceptibilities are divided based on the amount of ferro- and/or ferri- magnetic minerals within the rock structure. While ferromagnetic materials have the highest susceptibilities, they do not occur naturally on the Earth's surface (Burger, 1992). Thus, they are not usually considered, except in special cases of meteorite impact areas. In general basic and ultrabasic rocks have the highest innate susceptibilities, igneous and metamorphic more intermediate, and sedimentary rocks generally having lower susceptibilities (Reynolds, 1997). The main magnetic mineral is magnetite, but pyrrhotite, ilmenite, and titanomagnetite can also hold magnetization (Burger, 1992). Magnetite is the primary magnetic bearing mineral species of the rocks measured in the 98th street borehole paper (Hudson et al., 1999), and is thus believed to be the primary cause of magnetic anomalies in this study. The 98th street borehole is located in the central area of the Albuquerque Basin. The paper characterized the magnetic properties of much of the Santa Fe sediments predominant in the basin. Magnetite is derived from exposed crystalline basement and volcanic rocks around and within the Albuquerque Basin (Grauch et al., 2001). Erosional processes can spread the magnetite out throughout areas of the basin and into various sedimentary depositional units. A combination of Hudson et al. (1999), Hudson and Grauch separate field observations (Grauch personal comm., 2001) of susceptibility data measured on samples of various units of the Albuquerque Basin was used to constrain possible susceptibilities for depositional units in the Sand Hill fault zone.

III. Geological Setting

The Sand Hill Fault is located approximately 20 miles northwest of Albuquerque, within the Arroyo de la Calabacillas quadrangle in central New Mexico. It is one of the major north/south trending normal faults bounding the western margin of the Albuquerque Basin, approximately 9 kilometers in length (Heynekamp, 1998). The Sand Hill Fault is a growth fault that juxtaposes synrift sediments from the Pliocene-Pleistocene upper Santa Fe group against middle Miocene to Oligocene lower Santa Fe group rock units. The displacements on this fault range from ~10m to ~600m down dip (Rawlings, 2001; Hynekamp et al., 1999). The Sand Hill Fault is well exposed to the west, due to the badlands topography of this area. It has been extensively geologically mapped and studied; hence, it provides good geological constraints for model aspects of this research (Cather et al., 1997; Hudson et al., 1999). The mapping of this fault is detailed, including relative positioning of the fault structures that were able to be mapped in the field (Cather et al., 1997).

Both the Sand Hill Fault and Albuquerque basin are part of the larger Rio Grande Rift feature. The Rio Grande Rift is one of the major continental rift structures in the world. It extends for more then 1000 kilometers from central Colorado to northern Mexico and parts of Texas and New Mexico (Hawley et al., 1995). A thin, brittle upper crust and a ductile lower crust characterize the Rio Grande Rift. Magmatism is very prominent in areas of the rift structure. Faulting is prominent in the areas in and around the rift structure, creating various grabens and basins. The Albuquerque Basin is one of the largest and deepest basins of the Rio Grande Rift. Thus, the sediment fill of the

Albuquerque Basin and the subsequent faulting structures within the fill has been studied extensively (Hawley et al., 1995).

The smaller scale fault structure is documented well in Heynekamp et al. (1999) and Rawlings (2001). The fault dip varies from 70 E to near vertical along the strike of the fault. The fault consists of a damage zone, mixed zone, and core zone (Heynekamp, 1998) (Figure?). The damage zone is defined as the first evidence of minimal deformation. These include deformation bands and bedding dragged up relative to the mixed zone (Heynekamp, 1998). Mixed zones are areas of intense deformation, where bedding has been overprinted or completely destroyed through processes of tectonic mixing. These mixed zones include dragged and extended bedding, multiple slip surfaces, and areas of intense tectonic mixing of sediments. Bedding drag can be so severe as to orientate thin beds to sub-parallel with the fault near the core zone (Heynekamp, 1998). Core zone is the area of maximum fault slip accommodation. The core zone is generally much thinner than either the damage zone or mixed zone. The overall degree of deformation increases as one moves from the damaged zones to the core zone. Bounding the damage zones on either side of the fault are the undeformed parent material rocks (Heynekamp, 1998). The fault zone widths are quite variable along the fault, ranging from 2.5 meters thick with poor cementation in the southern parts to as much as 20 meters thick and strongly cemented farther to the north (Heynekamp, 1998). Figure 2 shows two of the generalized cross sections of this fault at different areas from Heynekamp (1998).

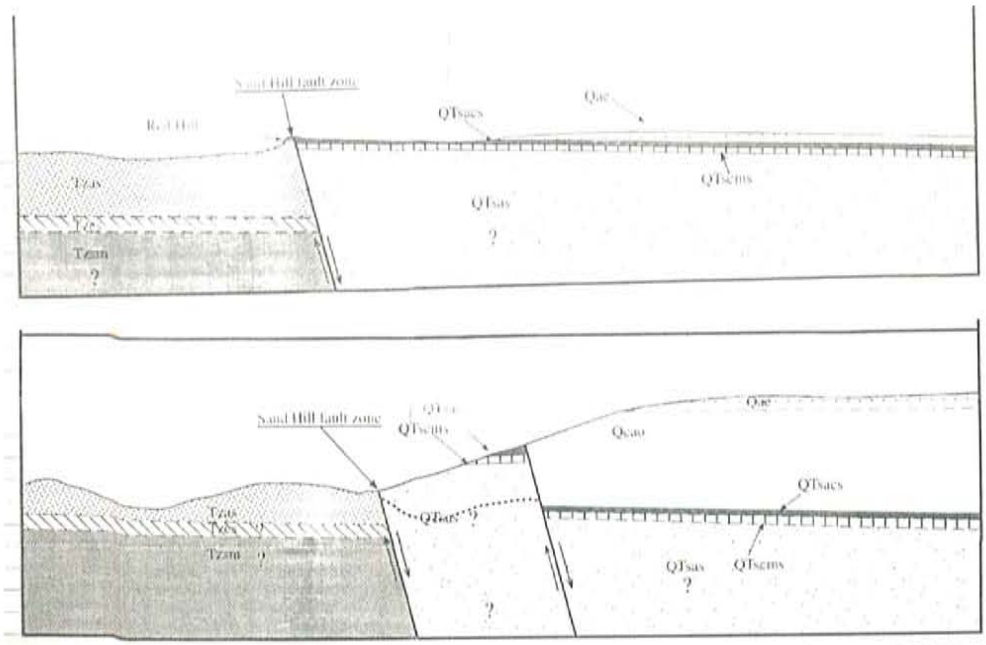

Figure 2. Two cross-sections from Heynekamp (1998). Both are in the general area of SHF7 line. Lines located on the left of both cross-sections are equal to 15 meters and there is no vertical exaggeration (Each cross section 650 meters long). Both cross-sections expose an area of approximately 100 meters on footwall. Units on the footwall of the Sand Hill Fault consist of Tertiary aged Lower Santa Fe group sediments (Zia Formation), hence Tzsm is Tertiary aged, Zia formation, sand-mudstone lithofacies. Units on the hanging wall consist of Quaternary-Tertiary and Quaternary aged Upper Santa Fe group sediments.

This variation is attributable to the amount of clay content in the layers juxtaposed against the fault. Sediments with high clay content act as lubrication for faulting mechanisms due to the clays shearing properties, thus keeping the fault zone localized with slip along the core zone. Thicker, sandier sediment packages become incorporated into the fault core and act to widen the fault zone, as the bigger particles are less conducive to the shear motions of the fault (Heynekamp, 1998). The correlation of the Zia formation bedding structure and fault zone width is documented in Heynekamp et al. (1998). Another important feature of this fault is colluvial wedges. These wedges come about from fault rupture that generally leaves the hanging wall block of a normal fault displaced lower then the footwall. The exposed opening on the hanging wall side of the fault is then filled in with incoherent and loose sediments, usually derived from the

footwall, whether by gravity, eolian deposition, or fluvial deposition related to the fault. Colluvial wedges produce distinct sediment packages that can be quite extensive in size due to extent of the continuous fault rupture movements along the fault. Estimates on the colluvial wedges at the Sand Hill Fault range from a few meters to near 40 meters thick (Smyth, personal comm., 2002). Lateral estimates of some colluvial wedges have been up to 100s of meters away from the fault itself (Machette, 1978), but no estimates exist on the lateral extent of the colluvial wedges of the Sand Hill Fault. These colluvial wedges are important for paleoseismological dating on various faults and their unique arrangements could be prime magnetic signature targets.

The lithology of this area is quite diverse. The main units that are exposed in this area consist of the lower Santa Fe formations, upper Santa Fe formations, and various Quaternary sediment covers. The Santa Fe group is loosely defined as the sediments that fill the Rio Grande Rift. The sediment units range from around 1000 meters thick along the basin margins, to 5 or more kilometers thick in the central basin. The time of emplacement ranges from 0.5 million years ago to 30 million years ago (Hawley et al., 1995). The whole Santa Fe group is divided up by two unconformable boundaries. The lower Santa Fe group consists of the Zia Formation. This formation is exposed only in the footwall of the Sand Hill Fault. Estimates place the Zia Formation at approximately 200 meters thick in this area, but it is not fully exposed (Heynekamp, 1998). The upper Santa Fe group consists of the Sierra Ladrones Formation. The lower and middle units of the Sierra Ladrones are found only in the hanging wall. The upper most unit of the Sierra Ladrones has been mapped on both sides of the Sand Hill Fault. At its largest exposure,

this Sierra Ladrones formation measures approximately 50 meters thick (Heynekamp, 1998). Below the sediments, older Mesozoic and Paleozoic rocks exist, some 300 meters or more below the surface (Hawley et al., 1995). Figure 3 shows the larger scaled cross section of the Albuquerque Basin, including Sand Hill Fault of Hawley et al. (1995).

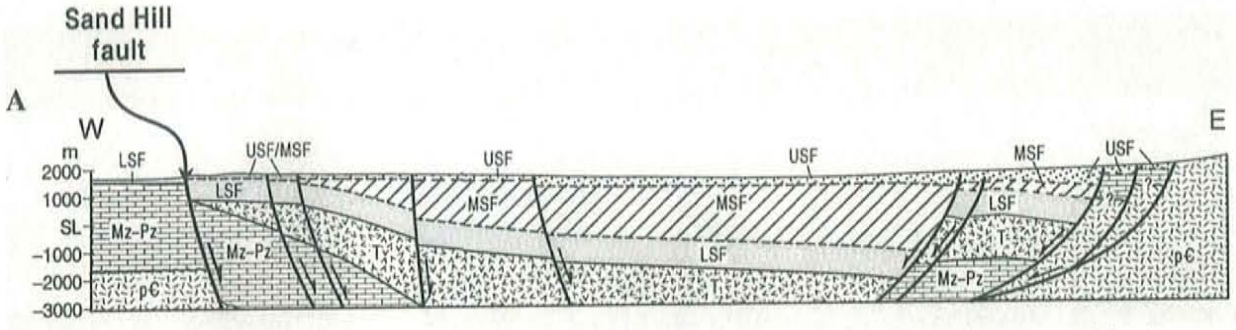

Figure 3. Cross-section of the Albuquerque Basin from Hawley et al. (1995). Sand Hill Fault position is to the left. Units are USF = upper Santa Fe Group, MSF = middle Santa Fe Group, LSF = lower Santa Fe Group, T = Tertiary volcanics, Mz-Pz = Mesozoic-Paleozoic, pC = Precambrian.

IV. Methods

A. Equipment

This project involved a variety of equipment and software applications. The major parts of this project involved the magnetometer used for data collection and the modeling software. These are covered in some depth, with some mention of additional applications and procedures as necessary.

All of the magnetic data was collected with a Geometrics G-858 cesium procession magnetometer. The unit consists of a belt-mounted display/logging console. The console connects to the cesium sensor, which is attached to a hand-held counterbalance staff (Geometrics, 1995) (Figure 4).

Figure 4. Geometrics G-858 Magnetometer

(Geometrics, 1995). Both the battery pack and sensor connect to the console. An additional sensor connector is available for gradient operation and an I/O port for data download and GPS input (Geometrics, 1995). Neither gradient, nor automated GPS input, were used for this survey.

For this survey, the sensor was held approximately one meter in front of the surveyor and one meter from the ground. Data was logged with time stamps for each reading. Data was also displayed on the console unit to facilitate in-field data quality

control. Sampling time was a reading every 0.2 seconds, this gives a sensitivity of 0.03nT variation per sample (Geometrics, 1995). Additional information on the G-858 can be found at Geometrics website www.geometrics.com or the G-858 user manual (1995).

The modeling for this project was done with GM-SYS, a program from Northwestern Geophysical Associates, Inc (NGA). GM-SYS is a program designed to calculate the gravity and magnetic response from a geological model and comparison to collected data (NGA, 2001). The program can be used for forward or inverse modeling. Inversion techniques were not utilized, since inversion requires a very strong amount of a priori knowledge, without which models are purely left up to statistical analysis (Gibson and Millegan, 1998). With general knowledge of the area, the best approach is forward modeling (Grauch, personal comm., 2001). Forward modeling allows a user to input the model every step of the way, making changes as need be to best-fit observed data and modeled response (NGA, 2001). The program starts with two generic blocks, an air and a crustal rock block. Each block is tied to "infinity", or +/- 30,000 kilometers to reduce edge effects from sharp boundary cut offs (NGA, 2001). The user inputs additional information, including topography along profile, the magnetic field, inclination, and declination for the day of data collection, and observed data. Various block-like models are constructed by the user to simulate geology within the area of study, each with a unique user supplied magnetic susceptibility value. The program calculates a response to the various defined geological models and utilizes a DC shift to match the modeled response with observed data (NGA, 2001). The magnetic response is calculated based on

the methods of Talwani and Heirtzler (1964), using the algorithms of Won and Bevis (1987), and proprietary methods of NGA to speed up and increase efficiency of the calculations (NGA, 2001). Users then can manipulate model parameters (block properties) until a suitable RMS error fit between observed and modeled responses is obtained. The geological reasonability of these models is left to the modeler's discretion.

Additional instrumentation used included a Trimble Global positioning systems unit. Additional software included Microsoft Excel, Matlab, Geometrics MagMapper v2 software, and NGA Geomagnetic Reference Field (NGRF).

B. Procedure

Before collection of data began, the Cather et al. (1997) mapping of the Arroyo de Las Calabacillas (former Sky Village S.E., quadrangle) was overlain onto the USGS aeromagnetic map of the area to be surveyed. Aeromagnetic anomalies were highlighted along the quadrangle to obtain relative relations of fault, anomaly, and map positioning (Grauch, personal comm., 2000). Ground lines were planned out to cross both the complete anomalies and fault structures. Extending the profiles to a minimum of 50 meters off of either side of the anomalies was desirable to obtain the complete anomaly shape. As this area develops into badlands topography to the west of the fault and the presence of man-made obstructions in areas east of the fault, a 50-meter buffer was not always obtainable to both sides of the anomaly.

In the field, a line was walked in an east-west direction, using GPS to maintain the east-west orientation of the lines. Field observations were also made (where geology permitted) to ensure lines crossed fault structure in the field. Line lengths, ranging from 360 meters (SHF1) to 840 meters (SHF4), depended both on anomaly size and accessibility due to topography. In all but two instances (SHF3 and SHF4 with variations of approximately 10 meters), north/south variations in the lines were less than 5 meters. Flags were staked every 30 meters along the line, to be used as visual guidance for walking the lines and user input marks into the magnetometer. For each line, the number of marks should equal the number of total flags laid down. This provided an infield check to assure lines were run accurately and consistently throughout each survey area. Marks were stored as special lines of text output by the magnetometer, which can easily be identified in spreadsheet output of the data.

The G-858 unit was run in simple survey mode. Marks were placed at each of the flags along the line. Two lines were collected at every site, an east-west run and a west east run with a continuous survey recording every 0.2 seconds. The duplication of data was used to correct spurious data along a line. GPS data was collected simultaneously along the line walks. GPS data was stored separately from the magnetics data. Time stamps in both sets of data were used for correlation in the lab.

After collection of two sets of the line, the flags were then picked up from the field. GPS positions of each flag was taken and transcribed into a field notebook. Areas of potential data problems were noted, such as drainage ditches or smaller arroyos

outwash. Fault structures noticeable at the field sites were positioned with GPS and photographed for later discussion.

Field data from both the magnetometer and GPS were downloaded to a computer. Geometrics MagMapper v2 software was used to edit the raw magnetometer data. General editing consisted of interpolating dropouts and despiking anomalous magnetic spikes, both automated procedures performed by MagMapper software. Linear interpolation of dropout removes all unrealistic null or zero values recorded in the field. The despike procedure removes spikes above 1000nT interpolated with surrounding points (Geometrics, 1995). Magnetic data was then converted to ASCII files and loaded into Microsoft Excel. The magnetic data information at this point included magnetic value, date, and time. Special lines of text were included in the data where marks were taken in their exact times relative to the machine operation during collection. From the marks the position of flags were placed and linear interpolation was done between 30-meter marks. In spots where marks were missed or erroneously marked, the GPS values complete with time stamps were used to correct their positioning.

The data was then run through an upward continuation Matlab algorithm (Appendix A). The algorithm used the upward continuation Fortran code of the U.S.G.S. magnetic data processing software available via ftp at ftp://musette.cr.usgs.gov/pub/pf/. The script reads in the easting position and magnetic value, filters the data down to one thousand data points, and interpolates the corresponding eastings. Once a thousand data points are set, a regional linear trend is removed from the data. After detrending, the data is padded with one thousand zeros to avoid wrap around effects when using Fourier

transforms to map the magnetic data to the frequency domain. Data is then multiplied by the exponential smoothing function from the USGS code. The exponential is a function of d, where d is the distance to be continued, negative for upward and positive for downwards. The output then was the detrended, upward-continued up magnetic data with associated easting and northing values.

The upward continuation is a type of low-pass filter acting to reduce high frequency noise, especially close to ground magnetic noise, and pull out broader-scale, anomalous features from the data. In essence, it emulates what data would look like if it was collected from a higher observation point. Figure 5 shows continuation of the SHF4 data line. Five meters was used as the continuation height for this figure to show the relation to the true data. The green line represents the true data collected in the field, black line represents the Matlab continuation algorithm, and red line represents the continuation with edge effects due to lack of data padding.

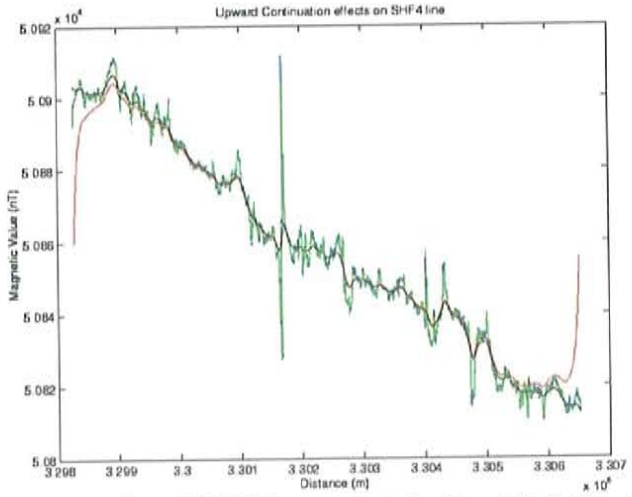

Figure 5. Five-meter continuation of SHF4 line compared with original data. Green line represents true data. Red line is the continued data with edge effects due to lack of padding. Black line represents upward continued data that has been padded.

Data can be upward-continued to any level. The initial continuation moved the data up to a height above ground of 100 meters, to mimic the U.S.G.S. aeromagnetic data collection height. The ground data was then visually inspected and compared to the aeromagnetic data for determining the relation of the two data sets. After comparison, the data is continued to a height of 80 meters above surface. This brings in more small-scale information, but does not overemphasize the anomalies with too much high frequency noise.

At this point, data files consisted of the continued magnetic value, northing, and easting. Corpscon was used to translate the GPS data collected in North American Datum (NAD) 1927 to NAD 1983. Data was collected in NAD 27 to be consistent with the Cather et al (1997) geologic map and the U.S.G.S. aeromagnetic data. Data was converted to NAD 83 to utilize U.S.G.S. 10-meter contour digital elevation models (DEM). The text files of magnetic data were input into ArcView 3.2, from ESRI. The northing and easting values were plotted overlain on a 10-meter contour DEMs. From the DEM, elevations were pulled associated with each northing and easting. The output data now included elevations. Data is then input into the magnetic modeling program, GM-SYS.

GM-SYS is a gravity and magnetics modeling application. To set up a model, the easting position, elevation, and the processed magnetic values were input into the program. After the initial model was set up, additional information was added, including the magnetic field values at that point and time on the earth, inclination, and declination.

Northing values are not needed, as the program assumes a straight line of collected data, and is incorporated in the user input of magnetic field values (which require the northing position). These values were obtained using NGA's NGRF, a geomagnetic reference field. Also, the height above ground of readings was set. In the case of 80-meter upward continuation, an elevation of 80 meters is set as the recording elevation within GM-SYS. Generalized block-like structures are used for the modeling procedure. Each block can be assigned a density and a magnetic susceptibility. Since the procedure is more adept at modeling generalized blocks versus smaller scale structures, bulk susceptibility values were used as an average of layer block susceptibilities. The susceptibility values used came from a variety of sources, including Hudson et al. (1999) and Hudson and Grauch separate field observations (Grauch, personal comm., 2001)

The process of iterative forward modeling is done until a reasonable fit of data and model response is obtained. This includes small-scale adjustments to the blocks, adjustments to susceptibility values, and adjustments to feature fault positions. Additional adjustments were made to the basic data input, including extending the elevation profiles by three times their true length. This was done to address the problem of edge effects that are produced where the true topography ends and the program adds a linear interpolation at each end of the topography to complete the basic block model (Figure 3). To account for this, a topographic profile that extended well past the ends of the collected data was needed. The decision was made to take the length of the collected lines and interpolate that length off both ends, as if the lines were continued on for three times the distance that they were. Comparisons were made between extended profile and

original profiles to detect the variations (Figure 6). From this procedure, it was determined that using elongated profiles was best.

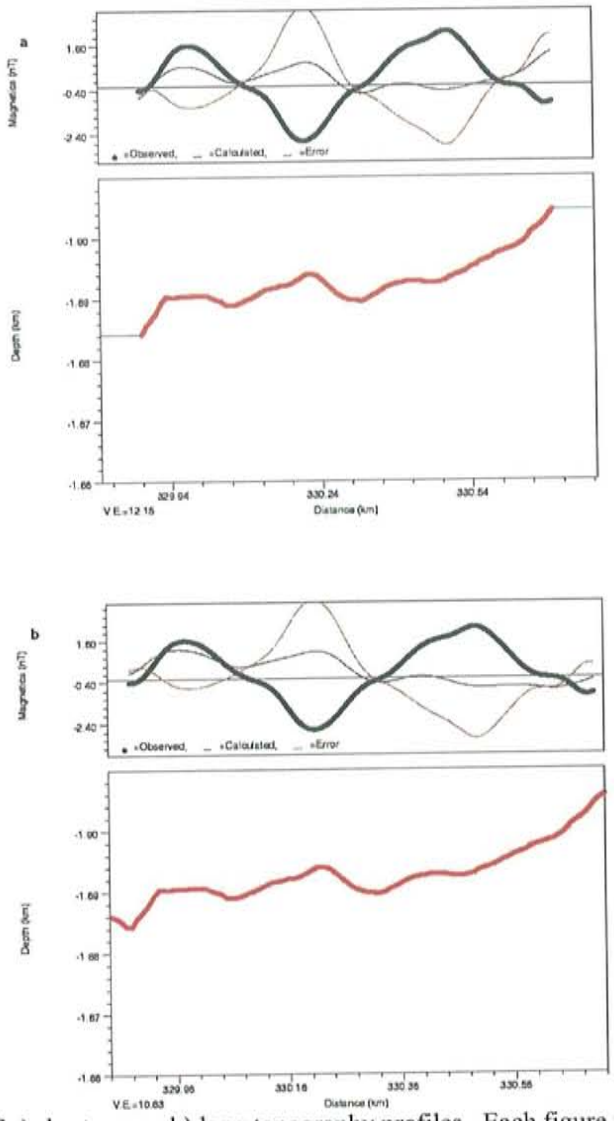

Figure 6. Comparison of a) short versus b) long topography profiles. Each figure is a model with a uniform susceptibility input below the topography. There is significant difference in model predicted from the topography of each (thin black line upper panel of each). Dark black line is the data collected in the field and thin red line is the variance of model and data in the upper panel of each.

As the 80-meter continued models began to fit well, 50-meter continued models were produced. These 50-meter models add smaller scale information not noticeable in the 80 meter. The same basic 80-meter models were used to get the general shape and model refinement was done to fit new inherent information. Thirty-meter models were

also made as the lowest elevation level of the upward continuations. Figure 7 shows the comparison of a) 80 to b) 50 to c) 30-meter continuations with trend removed. Visual inspection of 20 meters up, 10 meters up and at surface data were too noisy to accurately model (Figure 7d, e, and f). Sources of noise include at the surface magnetized rocks. As the scope of this survey was not to model individual rocks, 30 meters was used as the lowest point of observation.

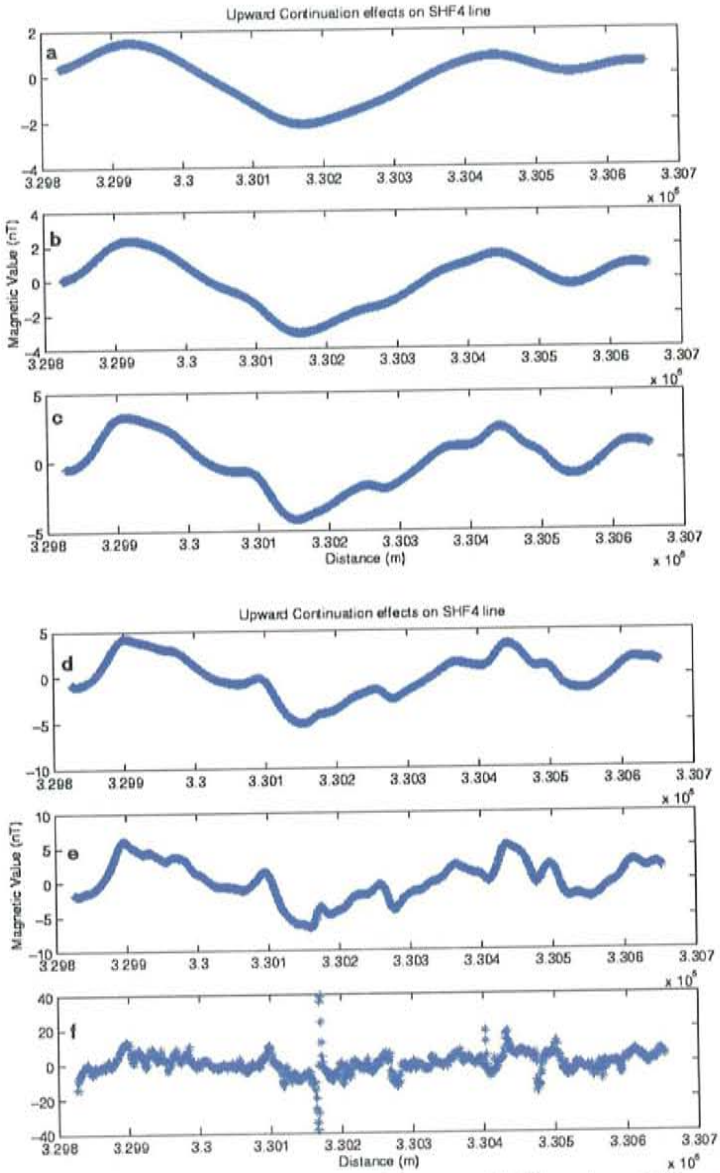

Figure 7. Various continuation levels on SHF4. a) 80-meter, b) 50-meter, c) 30-meter d) 20-meter, e) 10-meter, f) no continuation.

C. Data

All of the line data for the project was collected in the Arroyo de Las Calabacillas quadrangle. A total of nine distinct lines were collected. Two of these failed to cover the length of the fault and anomaly. Therefore, seven detailed lines are used in the characterization of this fault. The lines are labeled SHF1 through SHF7 (Figure 8) as they move south along the length of the fault exposed in the Arroyo de Las Calabacillas (former Skyvillage Southeast) quadrangle (Cather et al., 1997).

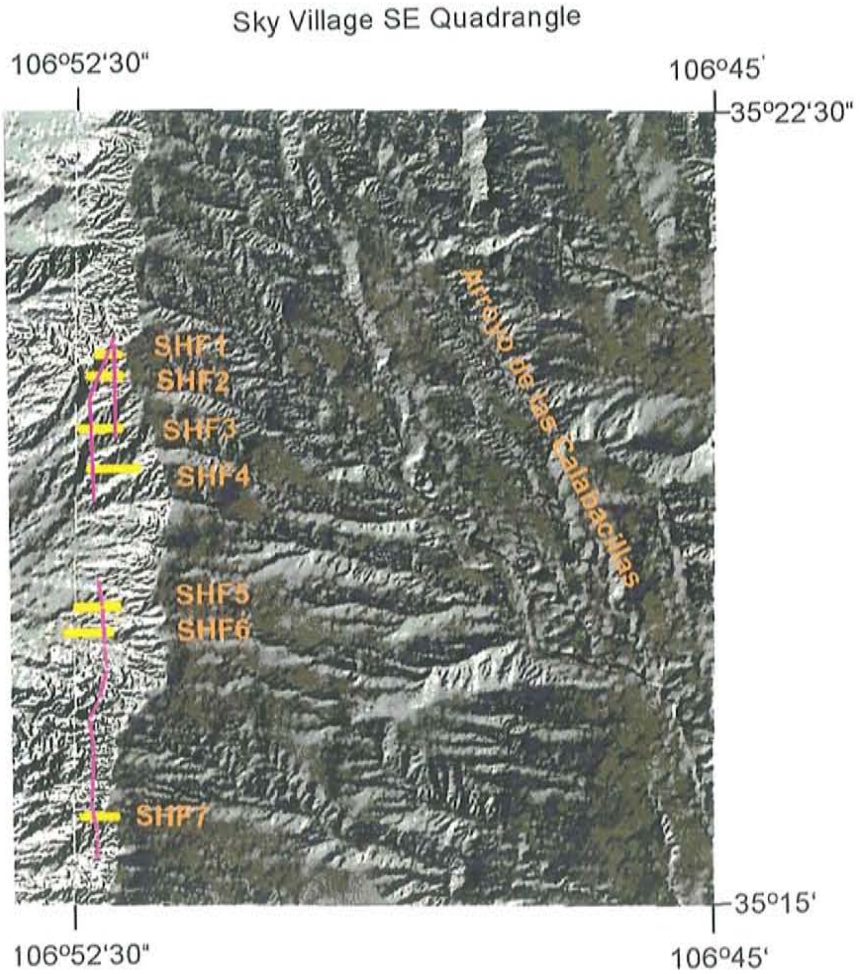

Figure 8. Sky Village SE (Arroyo de las Calabacillas) quadrangle with the seven magnetic lines (yellow) and relative fault position (pink) imposed from Cather et al. (1997).

SHF1 through SHF4 all were collected and referenced to the area of the Sand Hill Fault where no aeromagnetic expression existed. These lines have been placed from the uppermost bottleneck where the faults have been mapped to splay off from one another (SHF1). The sampling includes: SHF2, crossing over parts where both splays of the fault have been distinctly mapped in the field (Cather et al., 1997); SHF3, sampling across areas where both splays have only been inferred in the field; and finally SHF4, covering an area where only the western-most branch of the fault has been inferred, and the eastern most splay cannot be mapped or inferred due to lack of depositional contrasts. The SHF4 line was collected with the encouragement of Dr. Laurel Goodwin (Goodwin, personal comm., 2001), based on her thought that the eastern-most splay does not just die out, but can not be inferred at the surface.

The two lines SHF5 and SHF6 were collected over the central Arroyo quad anomaly. This anomaly was of particular interest due to the aeromagnetic anomaly being offset to the west in relation to the mapped fault. In this instance, the eastern-most edge of the anomaly starts at the mapped fault and extends from 100 meters up to 200 meters to the west of the mapped fault. This is different from the expected centering of the anomaly around the mapped fault structure. It is also noted that this area is covered with Quaternary sands, thus the fault has only been mapped where there are gaps in the Quaternary cover. As a result, a majority of the fault position in this area is interpreted. These lines are meant to clarify the position uncertainty in this anomalous area.

The final line discussed is SHF7. This area exhibits some anomaly offset from fault position, but also areas of anomaly centering on the fault. The anomaly appears to be slightly curved, convex to the west. Anomaly centering on the fault is near the central part of the curvature, while offset is at both ends of the curvature (Figure 9). SHF7 also has a bigger effect of badlands topography due to a closer proximity of the badlands, making line collection difficult.

Figure 9. Section of Aeromagnetic map showing the Sand Hill Fault and aeromagnetic anomaly. Cross in lower left hand corner is the bottom left edge of the Arroyo de las Calabacillas Quadrangle.

Each line site consists of two lines, an east to west running line and a west to east running line. This was done to provide redundant information in case of spurious data. In all but one instance (SHF2), both lines gave very similar anomaly patterns upon continuation. In the SHF2 line, the line that gave a similar signal to the aeromagnetic

data upon continuation up to the same level was used, based on the remaining lines being well matched to the aeromagnetic data.

V. Qualitative discussion on anomalies/data

A. Continuation effects

First, the various continuation levels and their effect on the data need to be considered. As expected, with increased distance away from the ground, data variability is decreased in the data set. A general comparison of mapped fault position from the Cather et al. (1997) map with the anomaly structure shows small features that appear to be related to the mapped faults, even if they do not cause the main anomalies. The appearance of these small-scale features decreases with increased elevation away from the fault in the continuation. Hence, the expectation is to deduce more information from the ground-based data as distance from surface is decreased (Figure 7). Another notable feature of the continuation is the decreased amplitude of anomalies with distance continued up. This is an expected situation as magnetic strength is inversely proportional to distance from source of anomaly. Figure 10 shows the decrease in anomaly amplitude with a continuation from 10 meters (a) above topography to 30 meters (b) above topography. The relation of anomaly to true collected magnetics data is also visible.

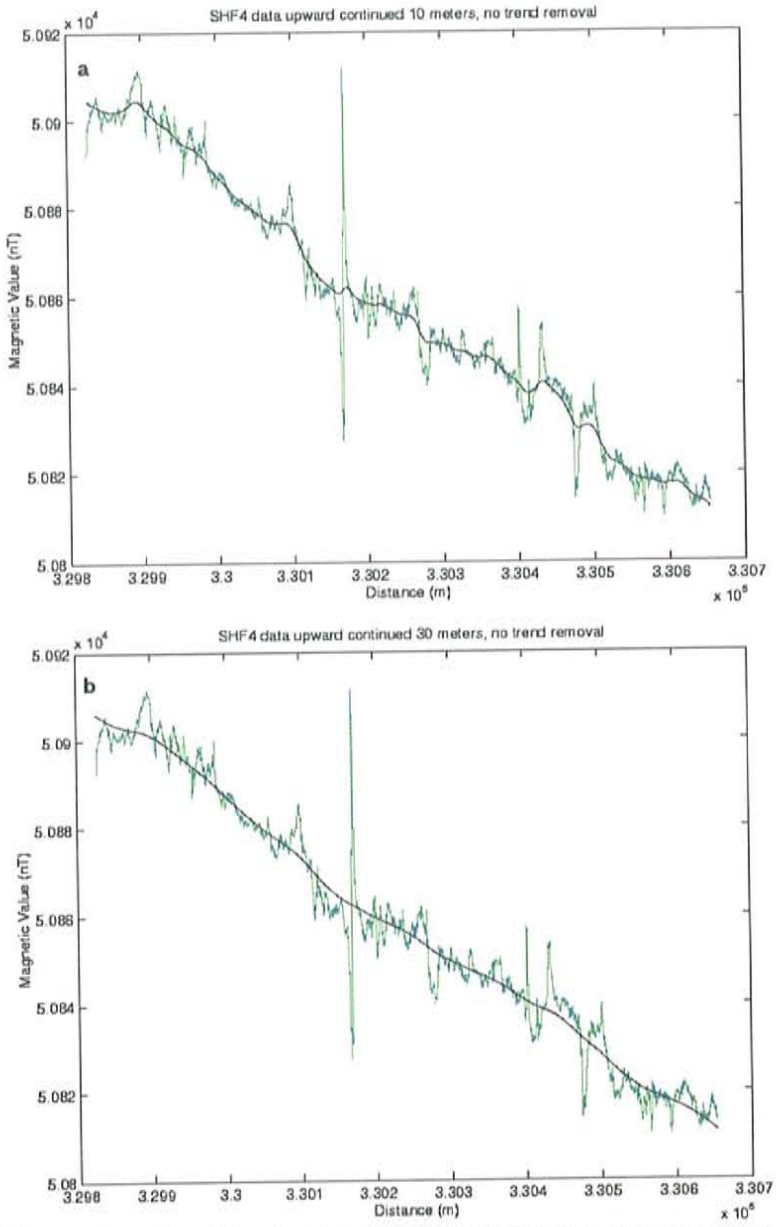

Figure 10. SHF4 data continued up 10 meters (a) and 30 meters (b). Trend is left in both profiles to show comparisons with original data.

B. Aeromagnetic versus ground data comparison

When a survey of this type is performed, general ideas about the shape and distribution of anomalies can be considered for a qualitative understanding of the data. This type of analysis can help with the modeling procedures and general understanding of the project. The first procedure performed in this analysis is comparing results to

existing data. To this end, the groundbased data was continued up to an elevation of 100 meters and overlayed on plots of the USGS aeromagnetic data collected at approximately 100 +/- 15 meters above ground (Figure 11).

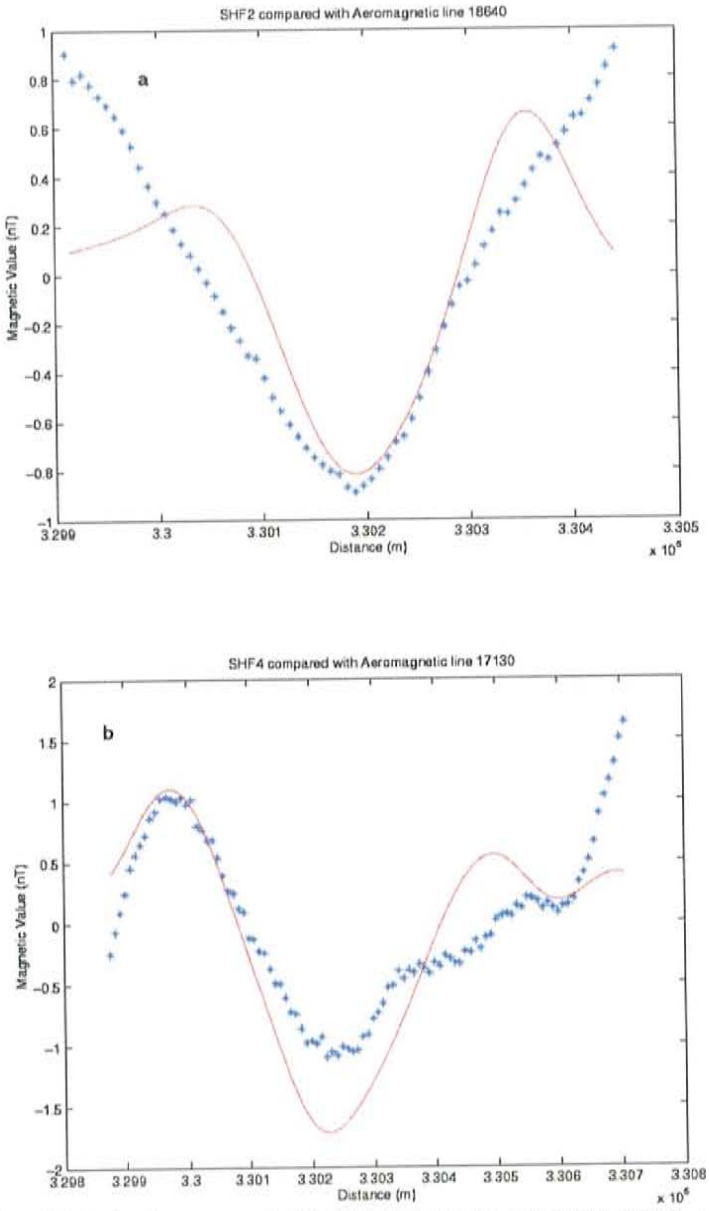

Figure 11. Ground based data (red) compared with USGS Aeromagnetic data (blue). a) SHF2 data, b) SHF4 data. USGS lines were collected at 100 meter spacing, thus exact lines that cover ground lines were not obtainable and closest related lines were used.

The ground versus aeromagnetic data comparisons give insight into both the quality of ground data and the consistency of the subsurface anomalies. In all but one instance, the basic anomaly shapes were very similar. Variations in relative anomaly amplitude and smaller scale features in the ground data are expected due to the differences in survey style.

C. Anomaly pattern discussion

Two dominant anomaly patterns appear in this survey. Five of the lines exhibited a similar pattern (SHF2, SHF3, SHF4, SHF5, and SHF6). This pattern consisted of an anomalous trough, surrounded on either side by peaks and declining off slightly at the ends of the anomaly (Figure 12).

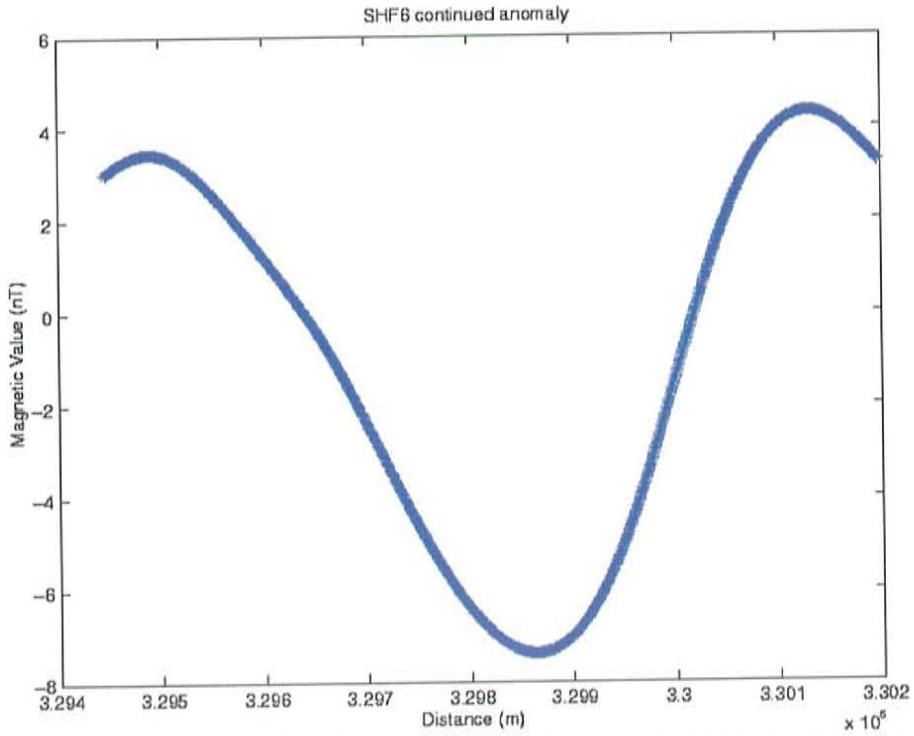

Figure 12. SHF6 line shows the anomaly shape prevalent in lines SHF2-SHF6.

The other two lines (SHF1, SHF7) had slightly similar general anomaly patterns. This pattern consisted of an anomalous peak in the middle and slight troughs on either side of the anomaly, which increased up slightly at the ends (Figure 13).

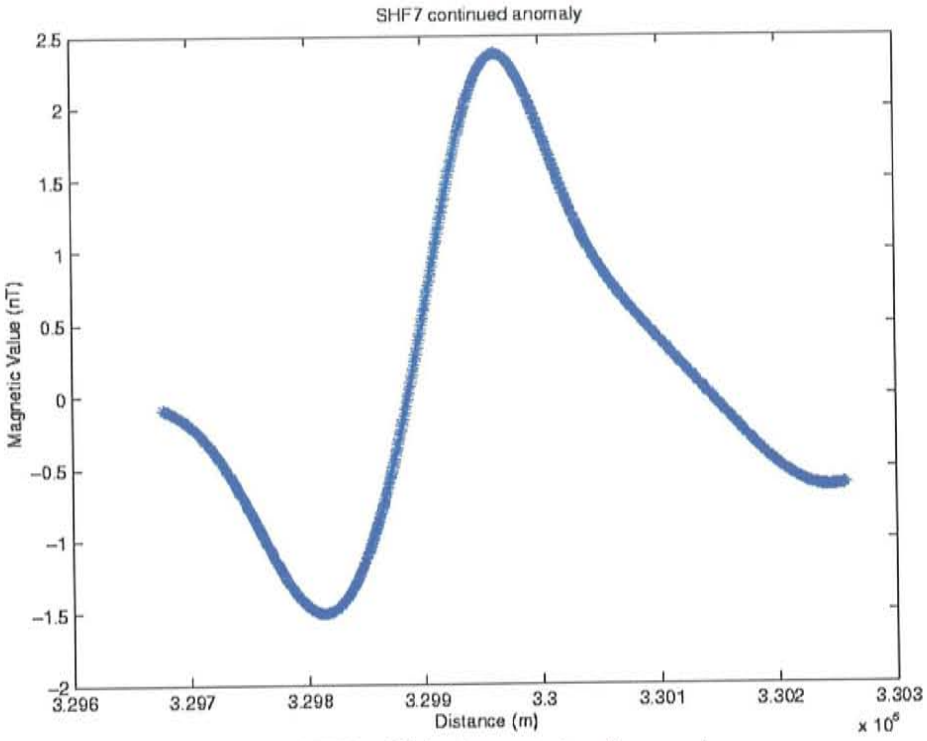

Figure 13. SHF7 exhibits the central peak anomaly.

Note that SHF1 is a symmetrical anomaly centered around the central peak, while SHF7 is asymmetrical. SHF1 and SHF7 were the northern-most lines and southern-most lines in this survey, respectively. SHF1 is located along the bottleneck of the two mapped faults by Cather et al. (1997) and general geologic appearances such as position relative to badlands topography seem to be significantly different between SHF1 and SHF7. Due to these geological and symmetry differences, SHF1 is considered separately from SHF7.

D. Anomaly spatial relation

Next we move to the question of how the anomalies are related spatially to one another. First, fault positioning relative to the collected lines is considered. Figure 8 shows the seven lines along the Arroyo de las Cabacillas, former Sky Village SE, quadrangle with the fault mapped as in Cather et al. (1997). The lines are divided into two distinct areas, a north section and a south section. The first area of interest includes the four lines, SHF1-SHF4. This is the area that bears no distinct aeromagnetic signature. Figure 14 shows the four lines plotted together from the north to south. Lines range from approximately 400 meters separation up to 800 meters separation from one another north to south. These four lines cover the extent of the mapped fault in this area with no anomalies in the aeromagnetic data. The variations in distance between the two mapped faults can be seen in the data. From just visual inspection of the anomaly pattern, the uppermost line (SHF1) appears to be the case of a single fault or two closely spaced faults. As the lines move south the anomaly peaks and the mapped faults space out farther from one another. In this view, the mapped faults and magnetic data appear to agree with one another conceptually. Marking the mapped fault position on each profile, there does appear to be a correlation of a fault located to the west of the anomalous troughs (Figure 14), in general agreement with the thick/thin models of Grauch et al. (2001). An additional secondary mapped fault lies to the east of the main trough feature in each line, although these features are only prevalent on the right-most trough of SHF1.

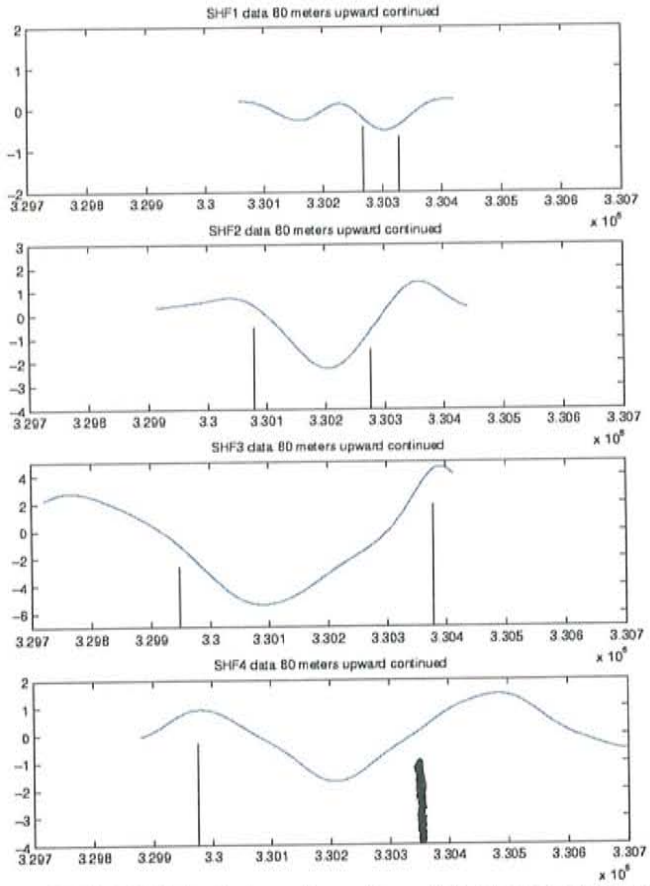

Figure 14. Magnetic lines SHF1-SHF4 in their north-south spatial relation with mapped faults of Cather et al. (1997) shown. Dark black line on SHF4 represents where fault projects from north, but no fault has been mapped or inferred for the second splay on that line. Magnetic Value (nT) on y-axis and distance (m) on x-axis.

The second area includes SHF5-SHF7 (Figure 15). All three of these lines were collected over areas that exhibit an anomaly in the aeromagnetic data. SHF5 and SHF6 are approximately 500 meters apart and cover the same anomaly, which was shifted relative to the mapped fault of Cather et al. (1997) in the aeromagnetic data. SHF7 is 3+ km south of SHF6 and thus the relation to the others lines is marginal. In this set, both SHF5 and SHF6 show the typical pattern with two peaks on either side of a trough, closely resembling SHF2-SHF4 data. SHF7 data is more similar to SHF1 data then the other five lines, with an anomalous peak in the middle of the line. Marking the relative spatial fault positions along these profiles, only shows a single fault splay to the

east of the trough features of SHF 5 and 6. While SHF5 and SHF6 appear to match the anomalies SHF1-4, there were no second faults mapped by Cather et al. (1997) in those areas. The SHF7 anomaly appears to be caused by features within the hanging wall side of the mapped fault (Figure 15).

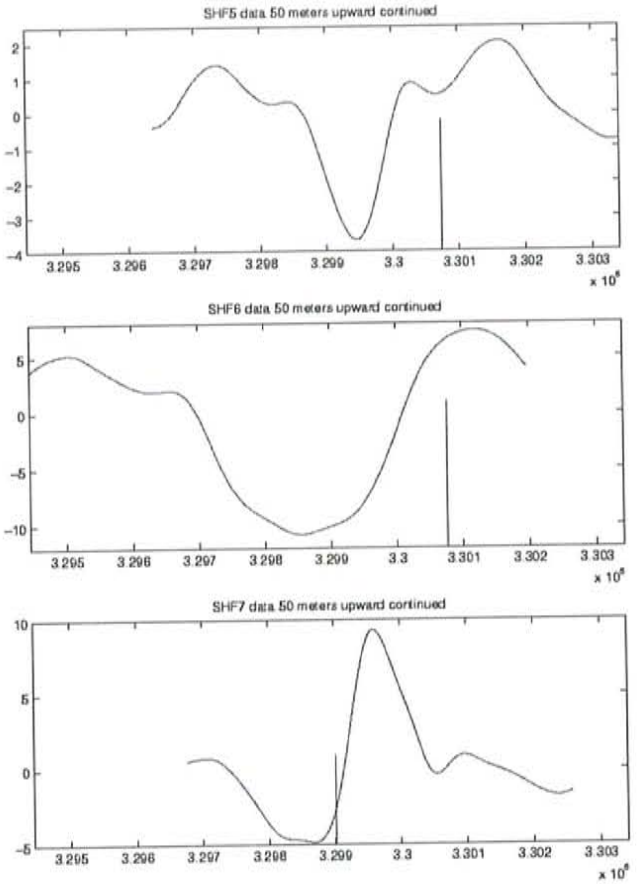

Figure 15. Magnetic lines SHF5-SHF7 plotted north to south with the relative fault positions emplaced. Fault positions pulled from Cather et al (1997) mapping. Magnetic value (nT) on the y-axis and distance (m) on the x-axis.

E. Qualitative analysis

In general, the data suggests that the aeromagnetic anomaly absence in the northern area of the Arroyo de Las Calabacillas quadrangle is simply due to anomaly strength. The anomalies in SHF2-4 are significantly lower amplitude then the anomalies in SHF5 and SHF6 (Figure 16).

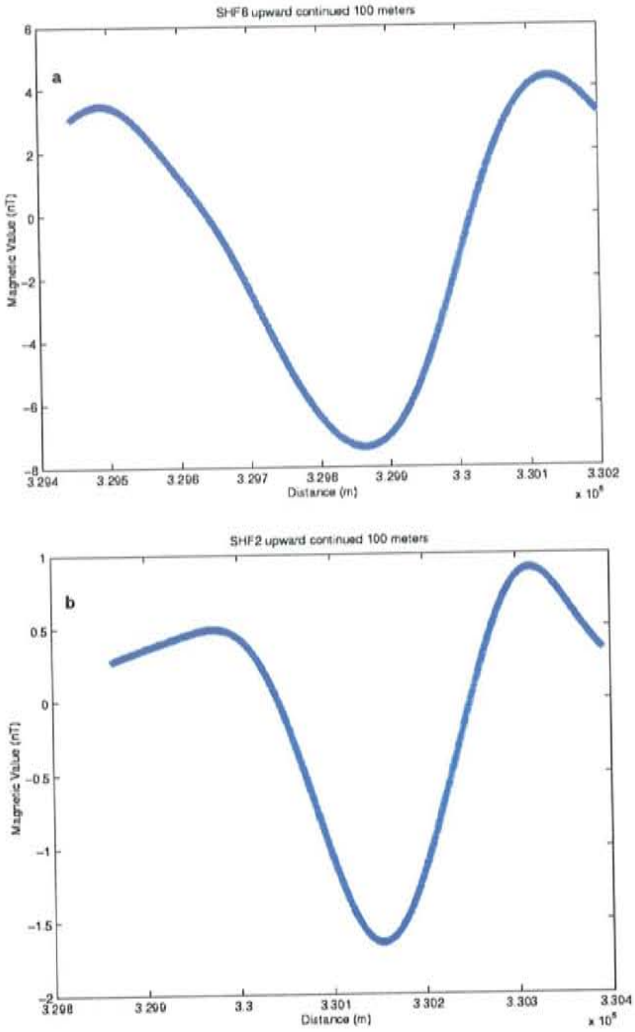

Figure 16. Amplitude relations of SHF6 (a) line in area with aeromagnetic signature, to SHF2 (b) line in area with no aeromagnetic signature. The vertical scale difference is important to note, as both anomalies appear very similar but very different in scale. SHF6 amplitude difference is approximately 12 nT, while SHF2 amplitude difference is approximately 2.75 nT.

All of these lines have the same basic anomaly shape, but with different amplitudes. In a large-scale aeromagnetics survey, the smaller amplitude anomalies are easily lost in application of contouring ranges. This is not the case in the area of SHF5 and SHF6 because the anomaly is bigger and stands out above the background in the aeromagnetic data. Thus, the obvious response as to why there is no anomaly in areas where there is mapped fault is due to the strength of anomaly, and not the lack of an anomaly. This

interpretation is strengthened by the fact that the same anomaly patterns of the ground-based data do, in fact, appear in the associated single lines pull from the related aeromagnetic data lines (Figure 11). Thus, the anomaly sizes seem to have been too small to be visible within the limits of the magnetic map contouring applications.

Another question that can be qualitatively addressed is the offset certain anomalies relative to the mapped fault position. In the SHF5 and SHF6 lines, where noticeable offset of anomaly is visible in the aeromagnetic signature, the general anomaly shape is similar to the northern lines, SHF2-4. In the northern area, there are two distinct fault segments that have been mapped or inferred in the subsurface. This suggests the presence of at least one additional, unmapped fault in the SHF5 and SHF6 line areas. Lines SHF5 and SHF6 are located on surfaces covered with Quaternary sediments which would poorly expose faults at the surface. The fault that has been mapped was only exposed in holes within the Quaternary sediments and inferred elsewhere. Thus, the presence of secondary faults in this area is not an unreasonable expectation.

F. Topographic effects

The questions of topographic effects on the data must also be considered. Elevations were extracted from 10-meter digital elevation maps (DEMs) to be most accurate. Anomalies were then modeled with the topography alone. In all but one of the

data sets (SHF7), some of the smaller scale anomalies do appear to be related to topography, but the main anomalous features appear to be caused by subsurface property variations. The SHF7 anomaly shows a possible correlation of the left trough anomaly with topography (Figure 17). Modeling is implemented later to further determine the possible relationships of topography to anomalies.

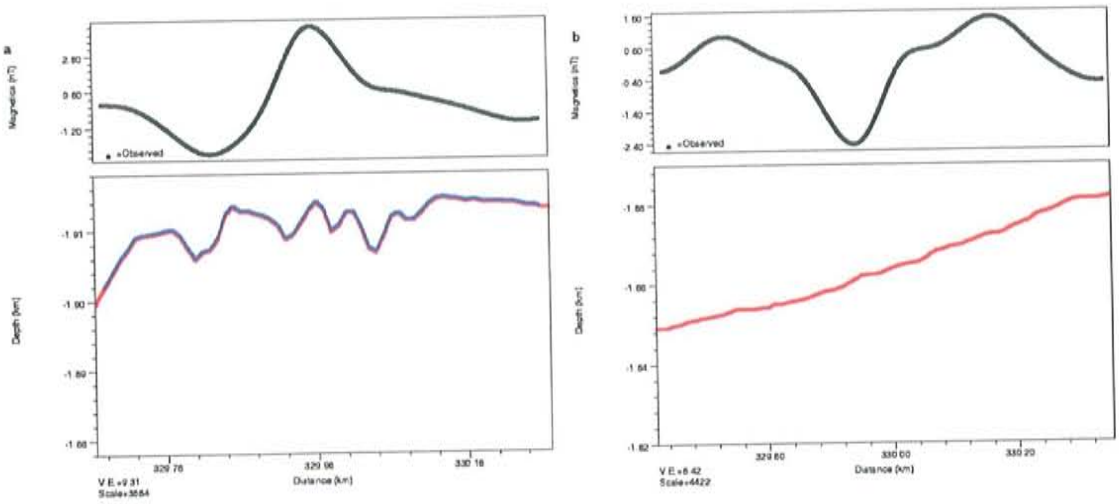

Figure 17. Anomalies with associated topography. a) SHF7 showing potential correlation of left hand trough and topography. b) SHF5 showing no correlation of topography and anomaly.

VI. Model Results and Discussion

A. Topography

It is beneficial to go from the least complex to the most complex model development. The initial phase of modeling in this project was based on topographic anomaly analysis. The simplest form of this comes from setting up the model with a uniform constant susceptibility through the entire subsurface. The higher susceptibilities produced more dramatic topographic effects. The anomaly that is produced comes

simply from the topographic profile directly under the collected line. These models showed some correlation with the collected magnetic anomalies, primarily at the outer edges of the models, but the main anomalies of no line could be attributed to topography alone. Each model is individually discussed later in this text.

The next question to arise was what type of anomaly does the topography produce if there is not a uniform block of susceptibility below, as is in the real world? As a complex understanding of susceptibility variation with depth and lateral changes cannot be achieved in an area like this, two model approaches were taken in attempts to model these scenarios. The first model involved placing a fault at its relative mapped position, or two faults in the case of lines SHF1 – SHF3. Susceptibilities were varied on both sides of the fault. The models used expected values from the Hudson et al. (1999), Tien Grauch and Mark Hudson (Grauch personal comm., 2001) field observations. Contrasts were varied based on visual inspection of best fit to models. Once a reasonably close fit was obtained, observations could be made on the relation of susceptibility contrasts in the subsurface as a cause for anomaly. Specific details are discussed later.

A second series of models were implemented. In these models, instead of making a fault, divisions were made at the relative lithologic contrasts in the subsurface. The estimations of lithologic contrasts were made from the Cather et al. mapping (1997). In all instances, some of the fault planes were included, as most areas of the fault were mapped due to lithologic contrasts at the surface. In areas where faults were just interpolated, the fault was still placed within the model, as a reasonable source of contrast

within the models. These models give more leeway to adjust relative susceptibility blocks along profile, as more lithologic contrasts then merely fault planes are allowable. The main assumption made in these models is that most of the magnetic anomaly is being produced in the near surface. Again models used susceptibility contrasts from Hudson et al. (1999), Tien Grauch and Mark Hudson field observations and susceptibility contrasts were adjusted by iterative forward modeling for best fit.

B. Simple Models

The next stage of modeling used susceptibility and offset contrasts between specific blocks within the subsurface. Models also included a uniform susceptibility value in the subsurface to account for topographic effects inherent in each model. Since magnetics is a non-unique method, the simplest possible models were constructed. The idea for how to set up these models came from Grauch et al. (2001). The thick-thin model concept seemed to best exemplify the anomaly patterns prevalent within the study, as in SHF2-SHF6, particularly the Figure 6c of Grauch et al. (2001). The thick-thin models involved a thin magnetic layer on the up thrown block juxtaposed against a thicker magnetic layer on the hanging wall. Thick-thin models are prevalent in growth faulting scenarios, with an accumulation of magnetic material on the hanging wall (Grauch et al., 2001). For the construction of these thick-thin models, an assumption is made that the main susceptibility contrast, defining the anomaly, is contained within a couple of definable layers. Thus the strength of the susceptibility contrast/offset of the

few layers juxtaposed against one another is significantly stronger then other contrasts along the fault plane.

With this assumption in mind, a series of models were constructed for the ground-based study. Each of these models contained a single fault that could reasonably match the ground anomalies. One notable problem that came about while modeling was the southward broadening of the anomalous features in the collected lines. In order to reproduce such broadening of the anomaly in the models, a combination of increasing the depth of the modeled (susceptible) geologic units relative to the topography in this area and increasing the thickness of the blocks is employed. In a larger scale geological sense, this implies that the main layer block contrast is covered by a thicker section of sediment fill, progressively in a southern direction. While this seems like a reasonable assumption, it must be noted that the overall elevation of the land is slightly decreasing towards the south. From SHF2, the elevation is 1,936 to 1,925 meters; to SHF4, which is 1,904 to 1,884 meters; to SHF6, which is 1,875 to 1,847 meters in elevation. Thus, the increased distance from surface to main blocks of susceptibility is not due to an increase in elevation, but rather a dipping down of the blocks in the southward direction. Also, the blocks that constitute the anomalies in the south are relatively thicker then the anomaly causing blocks to the north. As the Sand Hill Fault is a growth fault, both of these situations could be feasible, but do add some complications and strengthen the idea that a more complicated fault system is present. Inspection of existing geologic maps (Cather et al., 1997) are inconclusive as to supporting or negating these possibilities.

C. Furthering models

Through the simple modeling phase, it became apparent that some of the most simple models do no adequately model the collected magnetic data. The main problem came about tightening the trough of the anomalies on certain lines. Regardless the spatial relationships of the blocks to the surface, many of the modeled troughs were too wide to be a reasonable fit with data. Another problematic situation appeared in the modeling of different continuation levels. As the modeling moved from upward continued 80 meters down to the upward continued 30 meter models, more small-scale features were observed in the data that were most easily modeled with additional complex faulting. Thus, additional faulting was added to the models. Many of these secondary faults improved data fit greatly, with various positioning versus the main faults. Secondary faults were initially placed at the position of the mapped faults and adjusted accordingly to get a most accurate fit. These fault models mainly applied to SHF1 – SHF6, as SHF7 had a completely different anomaly pattern and is discussed separately. Additional adjustments were made and are described in each individual line discussion. In SHF1, SHF3, SHF6, and SHF7 only the 30 meter continued models are used in this discussion. In the remaining lines, 50 meter continued models were used in the discussion, due to strong of a presence of small-scale features in the 30 meter models to be accurately modeled. The following is that discussion of each line and details about their models. Relationships of each model to one another are discussed afterwards.

D. SHF1

This line was the northern most collected line. The topography only model used a uniform susceptibility of 0.001 SI units within the subsurface. Figure 18a shows the elevation only model. The topography seems to model the left side of anomaly well, but it does not match the central peak anomaly, nor the right trough anomaly at all. A higher uniform susceptibility enhances the difference between model and data, thus topography as the primary source of anomaly is ruled out. The next model constructed involved adding fault(s). To do this, faults approximating the mapped positions were added; for this particular line there are two mapped faults. These lines divide the entire subsurface block of the model. Dips of faults were used from nearest measurements, for SHF1 only then eastern-most fault splay has a dip recorded to it. This dip of 63° was used in both fault splays, as a best guess estimate on the western most splay. That dip of 63° is used on both faults in SHF1-SHF4. Susceptibilities are changed relatively within each of the three smaller blocks of the model created from the fault placement. Figure 18b shows the topography with the faults cutting through the subsurface. Susceptibilities were adjusted within the three smaller blocks of the model relatively to get the best fit to data. Both the ends of models generally correspond with the collected data, but again the central peak anomaly is not fit within this model at all.

A final model is created for these simplistic models. Divisions were made through out the model that are based on the lithological changes along the line. The lithologic units were relatively measured off of Cather et al. (1997) mapping. There are two main lithological contrasts along this line. One is approximately 100 meters east of the west end of the line. From the Cather map it is a change from a conglomerate-

sandstone to pure sandstone, both Tertiary in age from the Navajo Draw Member. While there is a general correlation between higher grain sizes and higher susceptibilities (Grauch et al., 2001; Hudson et al., 1999), this did not fit well along this lithologic contrast, as the peak is immediately to the right of the depositional contrast, thus it required the pure sandstone to have a higher susceptibility then the conglomerate-sandstone. The second contrast is located at the western-most mapped fault splay. Both sides of this contrast are sandstones. Thus a strong variation in susceptibility is not expected. There was no lithology contrast located at the eastern-most fault, as this fault was interpolated. This section of the fault is included in the lithology mapping, since the model becomes extremely skewed and misfit without it. This lithology model mostly correlates well with the data, but it is noted that the higher susceptibility is required in a wedge that would not be expected to be higher then the surrounded conglomerate-sandstone (Figure 18c).

The next iteration of modeling for this line involved actual faulted blocks. The first iteration was an attempt to fit a strongly magnetized dyke-like structure, primarily thought to be from remagnetization along the fault plane (Pierce et al., 1998), under the main peak. These attempts did not provide a good match of model and data; as well, they did not match up well with the mapped faults. A second attempt matched a thick-thin model on the eastern-most edge of the anomaly, as it could be related to the mapped faults and the topographic models seemed to fit the western-edges of the data. A model was constructed with a hanging wall block approximately 120 meters thick (0.0033 SI) and a footwall block of approximately 60 meters thick (0.0034 SI). The footwall block outcrops at the surface in the model, with the hanging wall being located approximately

40 meters deep (Figure 18d). The fault position is expected to outcrop near exactly where the western-most fault splay has been mapped in the field. Smaller additional adjustments were made with the model to get best fit, but nothing that is notable in terms of total structure. This model appears to be a good fit. There does not appear to be any more applicable smaller scale changes that can be made, for even the smallest change strongly skews the model. The eastern most fault is not required for a good fit.

From a geological perspective, this model fits the basic concepts of normal faults. It has a similar susceptible block offset. The thicker block is on the downthrown side of the fault and sediment fill is present throughout the area as is fits with growth fault type models, hence the use of thick/thin models. From the geological constraints (Figure 3) (Hawley et al., 1995), this model does seem to fit with the known mapped geology. The block would seemingly be of the Lower Santa Fe group, with upper fill being composed of middle and upper Santa Fe sediments.

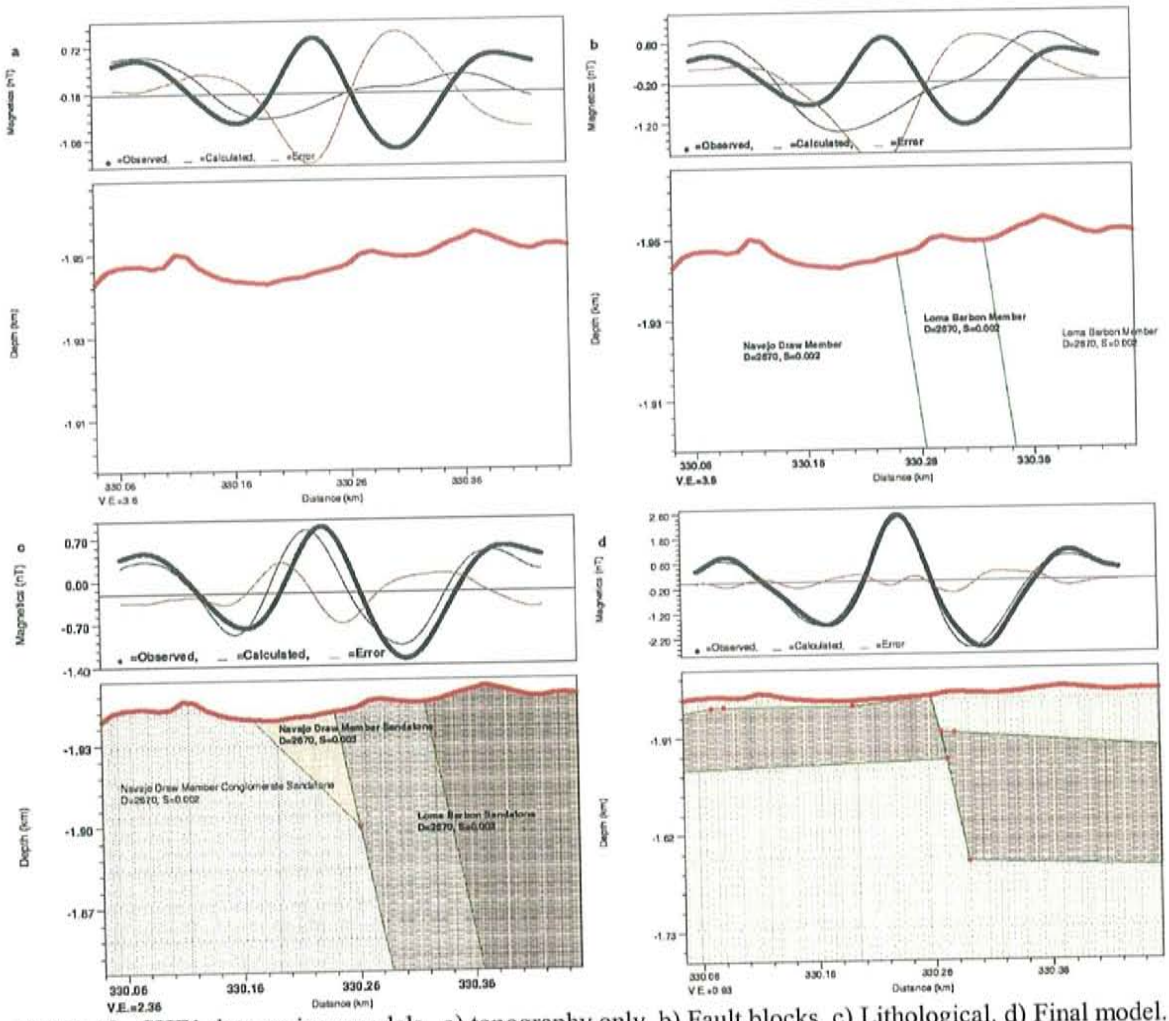

Figure 18. SHF1 data various models. a) topography only. b) Fault blocks. c) Lithological. d) Final model. Dark black line in upper panel represents data, thin black line is modeled response, and red line is misfit between model and data.

E. SHF2

This line covered an area where two splays of the fault have been mapped. The topographic model used two different susceptibilities. First a uniform susceptibility of 0.001SI is used (Figure 19a). The left side shows some correlation, but in general the data is poorly fit with this topography only model. As there intuitively appears to be a correlation of central trough and a trough-like feature in the topography, the susceptibility was moved up to 0.011 SI (Figure 19b). This was one of the highest susceptibilities

noted by Grauch (personal comm., 2000) around this field area. The higher susceptibility accentuates the features of the topography, yet is too high to assume to be the uniform susceptibility of this area. The model does show that the topographic trough can produced a similar anomaly to the collected data, yet the amplitude of the model anomaly is less then the collected data, even with a high susceptibility value. This model fits poorly elsewhere along the profile as well. The topography is not a significant source of anomalies here. Next fault positions were emplaced within the model and susceptibilities adjusted relatively in each newly created block (Figure 19c). A dip of 63° is used on both splays of the mapped fault, from the measurement on the eastern-most splay in this area. The right side of the model appears to match up relatively well with the data, but the left side does not correlate at all. This implies that the susceptibility contrast along the right-most fault in conjunction with topography match up well with the collected data, yet there is still bad misfit on the left side of the model. No lithology model was created for this line, as the only contrast exists at the western-most fault splay. The eastern-most fault splay has no mapped lithological contrast.

In general view, the SHF2 data appears to best be fit with a thick-thin model (Figure 19d). After this initial model was setup, it was apparent that a second fault was required to accurately model a strong peak on the eastern edge of the main trough. This fault offset a higher susceptibility (0.0035 SI) over the main faulted block. The orientation of this block is not clear; it appears to require an eastern dip. Once this was implemented, more small-scale adjustments were made, as the data had large amounts of small-scale information. The prominent feature on the western edge of the model seemed best modeled with a slight offset in the layer, on the order of 10s of meters, but keeping

the same susceptibility. This additional offset is thought to be minor complex faulting. It should be noted that this smaller offset is not required to match the general anomaly shape, but appear to fit the data best. Blocks ranged from 100 meters thick to 200 meters thick. The main contrasts all reside within the upper 100 meters of the surface with susceptibilities ranging from 0.0033 SI to 0.0035 SI. Again this model seemingly coincides with a normal fault model, similar susceptible layers offset with a thicker block on the hanging wall side of the fault. These layers seen to best represent the Lower Santa Fe unit blocks with overlain sediments being composed of middle and upper Santa Fe units.

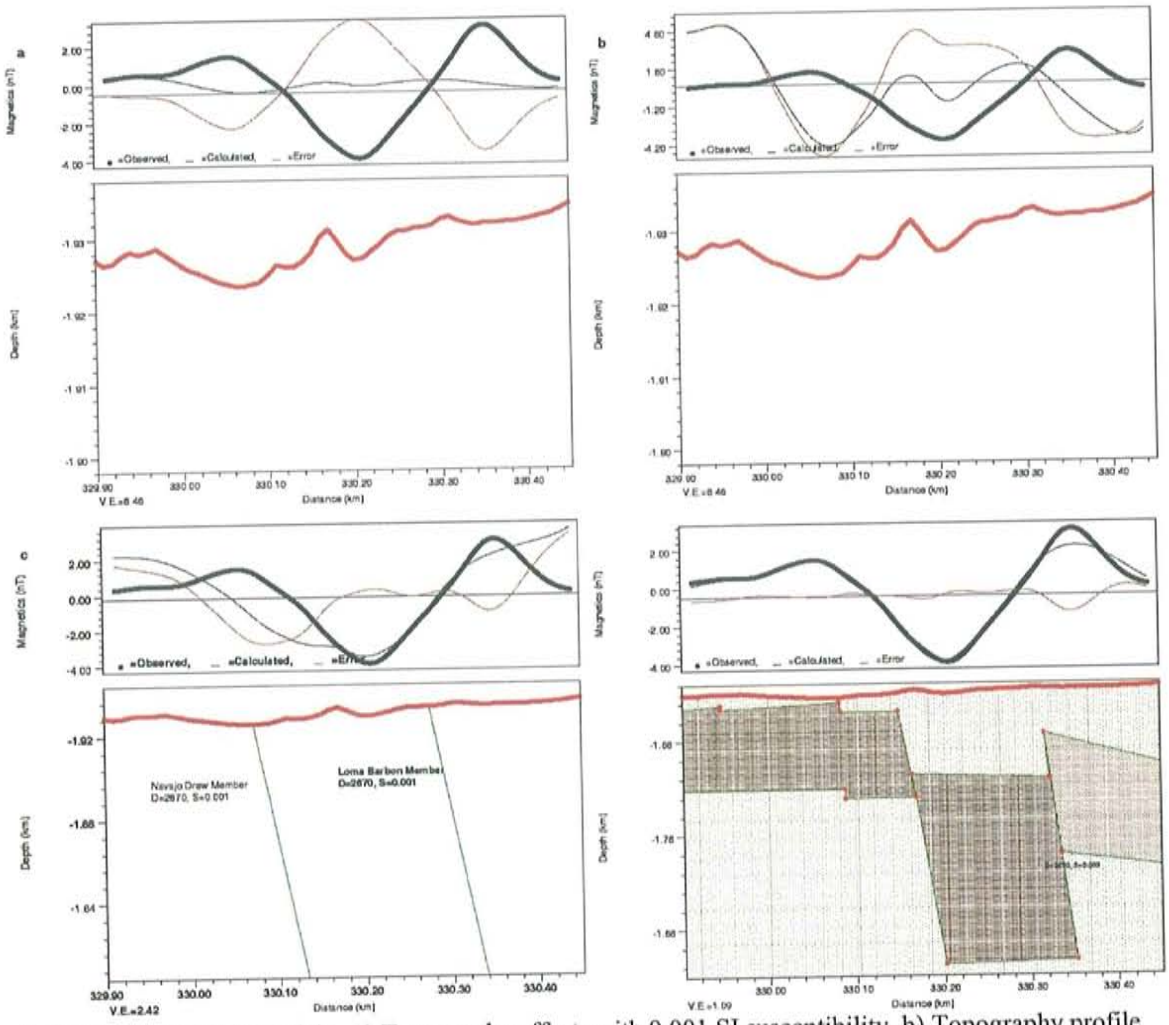

Figure 19. SHF2 data models. a) Topography effects with 0.001 SI susceptibility. b) Topography profile with 0.011 SI susceptibility. c) Model with fault blocks emplaced. d) Complex model to date.

F. SHF3

This line covered an area where the western-most splay fault was mapped, while the eastern splay had only been inferred. This line was also complicated due to a strong anomalous feature on the eastern most side of the line. This anomaly has a high-amplitude and low frequency and dominated the eastern end of the data collected. Field constraints prevented complete data collection across this anomalous feature. As the amplitude of this signal was quite strong and topography in this area was relatively flat, a topographic model with a uniform susceptibility of 0.001 SI showed no information. A

model was created with a susceptibility of 0.011 SI, again the highest measured value in the field from Grauch (personal comm., 2000) (Figure 20a). This model shows some correlation along the east side of the model, but little correlation elsewhere. Setting up the model with faults emplaced (63° dip on both splays) shows correlation with the general shape of the anomaly, yet the fit is still not very good (Figure 20b). No lithological model was created for this line, as the only contrast marked in the field is located at the western-most fault. The contrast is between sandstone overlain with Quaternary sediments next to exposed sandstone. The eastern-most fault splay has no mapped contrast.

This line had a large deal of additional complexity due to the strong eastern edge anomaly in the data, but this line still gives the similar anomaly type that is best fit with a thick-thin model (Figure 20c). The initial fault was placed along the western most mapped fault in this area. It fit the thick-thin model and matched up with the mapped fault well. It was apparent that a fault was needed on the eastern-most edge of the line to account for the huge anomaly spike in the data. This fault was placed in and adjusted for best fit, while it is in the general area of the second mapped fault in this area; it is not completely in line with it. This is expected due to the strength the anomaly has on that end and the continuation algorithms filtering out along that edge. The thick-thin model involved two blocks approximately 100 meters thick on the footwall (0.0034 SI) and ranging from 80 to 150 meters thick on the hanging wall block (0.0033 SI). To match the high bump on the eastern end, a high susceptibility, thick block needs offset above the secondary fault, approximately 170 meters thick (0.0047 SI). The main contrast is located within the upper 120 meters of the surface. A small adjustment was required at

the western edge of the model. This involved deforming the footwall block up some, to account for a small-scale feature in the end of the line. This is not assumed to be any type of faulting, rather just a feature of the layer in question or susceptibility distribution. The main contrast once again appears to represent a normal fault, with a similar susceptible layer being offset. Thicker block is present in hanging wall section, and both main contrasts appear to represent the Lower Santa Fe group. The high susceptibility block to the far east of the model is uncertain. This could represent a large deposit of Middle Santa Fe units, or a strong present of highly magnetized materials near surface. The topography along this area of the line has the highest elevations, some 20 meters higher then the western end of the line. A high susceptibility distribution along the surface could be a strong source of this anomaly. An oddly high ridge was noted in the field, approximately located where the data begins to strongly peak upward, but nothing definitive can be said for this area.

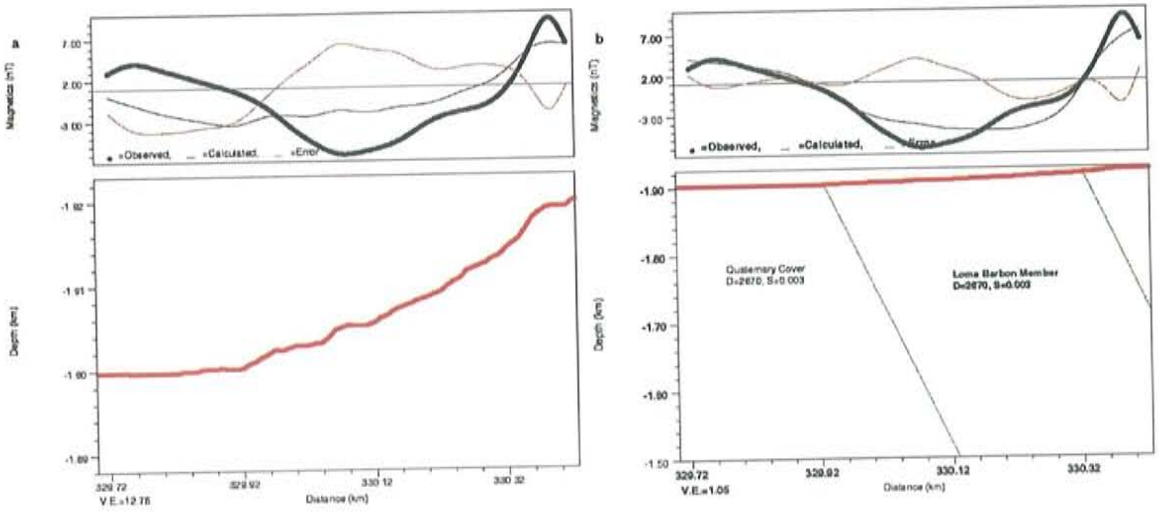

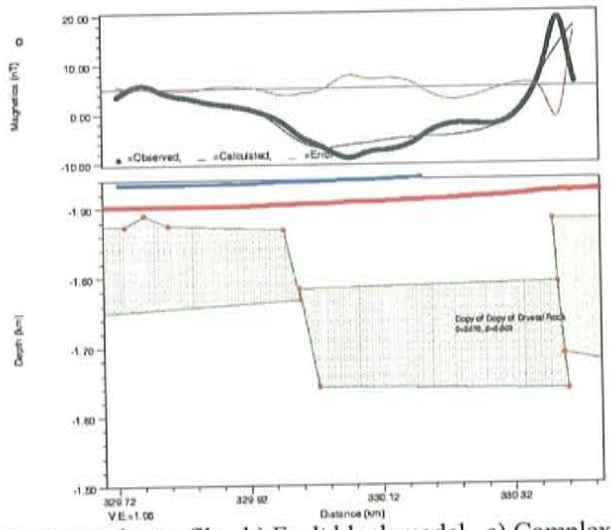

Figure 20. SHF3 data. a) Topography profile. b) Fault block model. c) Complex model to date.

G. SHF4

This line covered the area where the western most splay had been inferred and the eastern hand splay had neither been inferred nor mapped, but was believed to still be present by Goodwin and others who overtook the mapping project. For the topographic model, a susceptibility of 0.0025 SI was used (Figure 21a). This value best fit the data from visual inspection. The model shows decent correspondence on the far west of the model, but the main trough feature and eastern edge of the model are poorly correlated. This is apparent from a visual inspection of the topography, as there is a peak feature in the topography exactly where the main trough feature is in the data. A fault model (63° dip on both splays) was constructed (Figure 21b). Again the correlation of the model with the data is extremely poor, this line exhibits little, if any, effects of topography in the data. No lithologic model was made, as the only contrasts were located at fault boundaries.

As with SHF2, this data seemed best fit with a thick-thin model (Figure 21c). To correctly correspond a thick-thin model, this fault had to be placed within an area where no fault had been mapped. Upon general setup of the model, again a secondary fault was required to fit a high amplitude peak to the east of the main trough and to accurately model the width of the central trough. Once the secondary fault was emplaced, it did appear to line up in the general location of where we would expect the projection of the eastern-most fault splay to be. A third smaller fault line was required on the western margin to properly simulate another small-scale uplift feature in this model for the area. This fault did appear to generally correlate with the western-most inferred fault splay was located, but it was not a strong fit. The footwall of the thick-thin model is approximately 90 to 100 meters thick and 35 meters from the surface (0.0034 SI). The hanging wall is approximately 200 meters thick and located 100 meters from surface (0.0033 SI). The other subsidiary fault modeled required only approximately a 10 meter offset at the top of the block, but a 70 meter offset at the base, thus appearing to be a completely different layer juxtaposition next to the main layer in this model (Lower Santa Fe). This additional layer is thought to be part of the middle Santa Fe unit, but no specific determination can be made without an idea of which fault ruptured first.

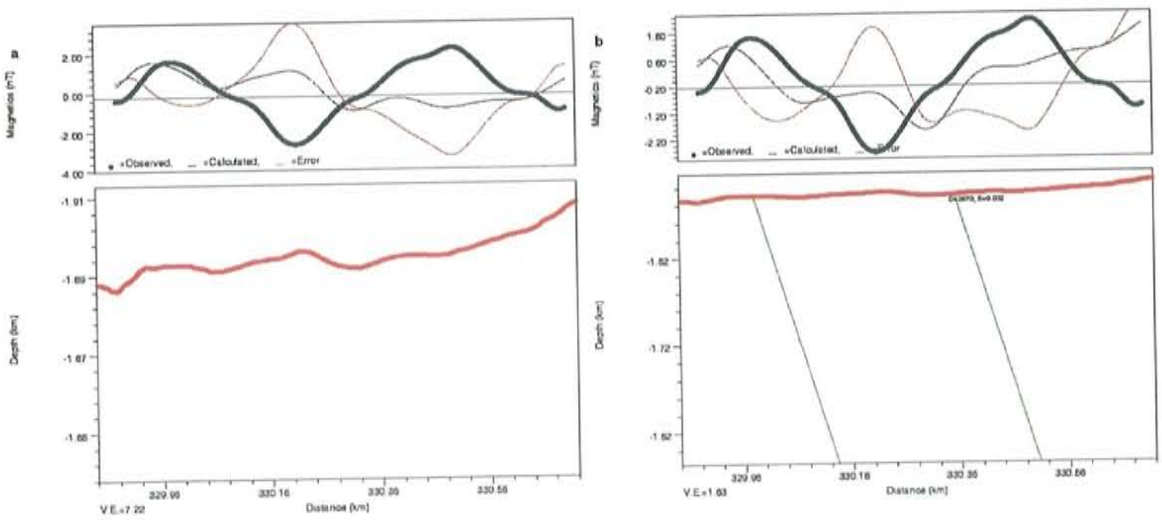

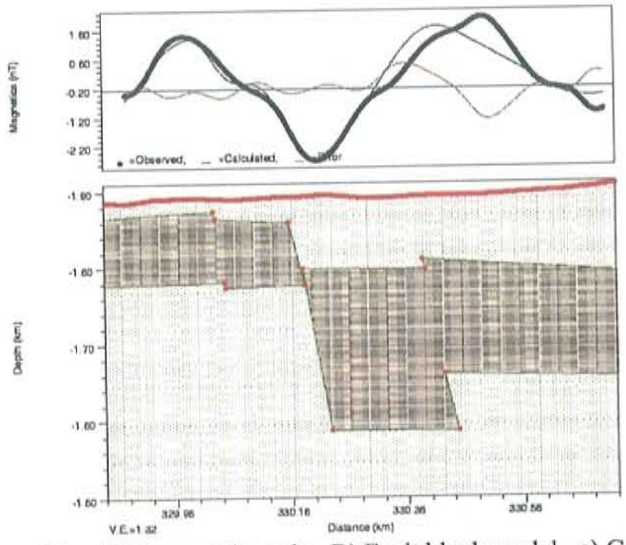

Figure 21. SHF4 data models. A) Topography only. B) Fault block model. c) Complex model to date.

H. SHF5

This line was over an area mostly covered in Quaternary alluvium. A fault splay had been partially mapped and mostly inferred though this entire area. Areas that had been accurately mapped were due to holes in the alluvium. The particular line was taken where the aeromagnetic signature showed offset from the mapped fault. The topographic model for this line used a uniform susceptibility of 0.003 SI. The model from topography showed little variation, as the topography is relatively flat lying (Figure 22a). None of the anomaly collected in this area appears to be caused by topography. The fault model for this line only included one mapped fault, even though the data collected for this line shows an anomalous signature similar to the previous lines which all had two mapped faults. A dip of 63° to the east is used on the fault, from one dip measurement taking in this area. The model with one fault does not correlate with the data well (Figure 22b). The one simple fault where mapped in the field is not the cause for this anomaly. The sites for SHF5 and SHF6 were mostly covered with Quaternary sediments, thus making lithologic variations very difficult to determine. Thus due to the extreme sediment cover, there was no way to determine orientation/dip of exposed rocks beneath. After a series of

lithologic models had been completed, it became apparent that no suitable model could be made that accurately modeled the exposed lithology, thus no lithologic models were used for this line.

Due to the extreme anomaly amplitudes, the fault block model for this line was quite complex in nature. It is fit with a basic thick-thin model, but required a great deal of additional complexity to get fits on much of the other information in the signal. This included three additional faults, besides the main fault for thick-thin modeling. Much of the smaller scale data in magnetic data appears to give credence to a more complex modeling system, with multiple fault units. All of the main contrasts to model this data are within the upper 150 meters of the subsurface (Figure 22c).

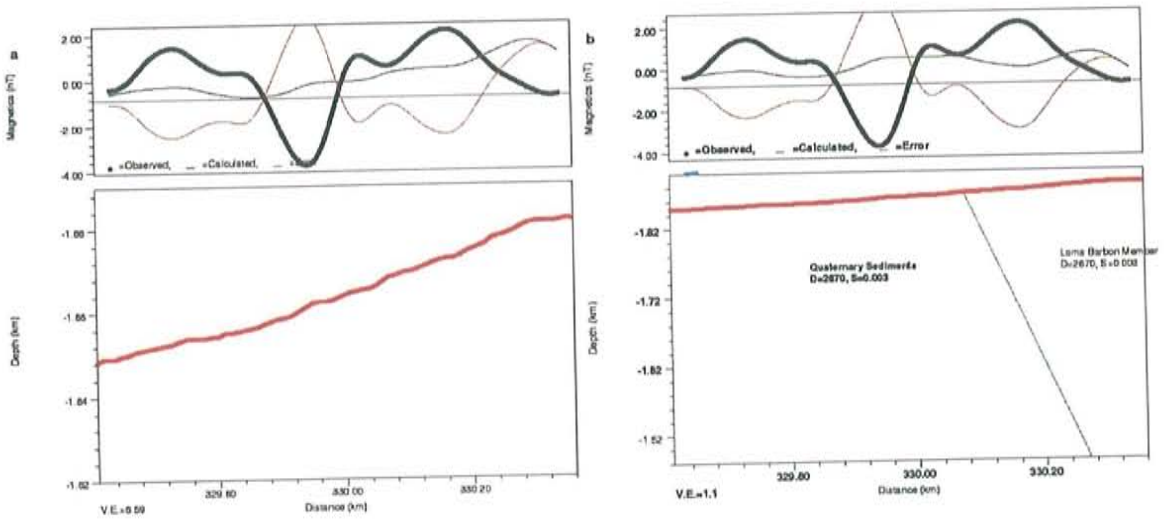

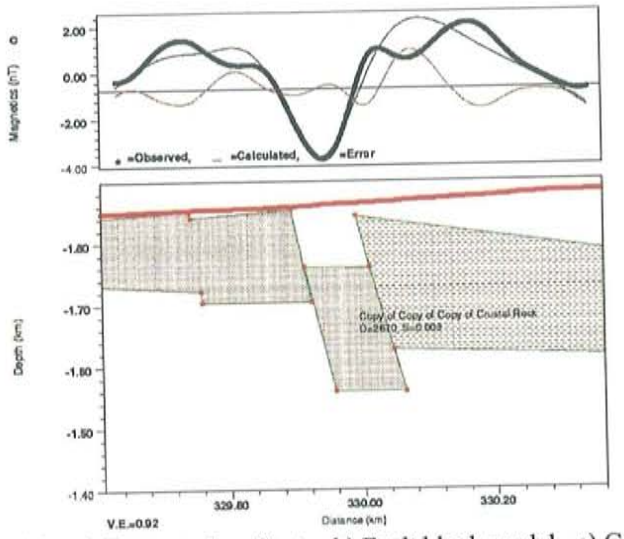

Figure 22. SHF5 data models. a) Topography effects. b) Fault block model. c) Complex model to date.

I. SHF6

This line, like SHF5, was in an area dominated by Quaternary alluvium cover. It also was collected over the offset aeromagnetic data area. The simple topography model for this line used a uniform susceptibility of 0.011, the highest mapped susceptibility in this area (Figure 23a). The high amplitude of the anomaly and the relative small changes in topography required the high susceptibility. A possible correlation exists at the west end of the line with a small bump in topography, but as a whole the topographic model and data are poorly correlated. For the fault model only one fault has been mapped in this area (63° dip on fault). As with SHF5, the anomaly on SHF6 appears similar to the previous lines which all had a second more western fault splay. Again, the one fault model for this area poorly corresponds with the observed data (Figure 23b). Only a small potential correlation exists on the western edge of this line. The same problems for the lithologic model of SHF5 apply to the lithologic model of SHF6. Due to extreme

amounts of Quaternary sediment cover, no orientation/dips of exposed rocks could be used to accurately make a lithologic contact model.

The anomaly amplitude in this anomaly was very strong, providing difficulty in modeling. With the qualitative look at the anomaly, the model was fit with the thick-thin model. An initial model is set with the thick-thin premise, but the fit was not good (Figure 23c). With a strong anomaly peak on the eastern edge of the line, a second fault was required. This secondary fault is in the general region of the mapped fault in this area, but it is not a strong fit between the modeled fault and the mapped. The high susceptible block on the far eastern end of the model is a bit anomalous. It could seemingly represent a section of middle Santa Fe unit, while the two main blocks of the thick-thin model are apparently Lower Santa Fe group rocks/sediments. The blocks varied from 80 meters thick to 180 meters thick in this model, with susceptibilities from 0.0033 SI to 0.004 SI. The main contrasts all resided within the upper 150 meters from the surface.

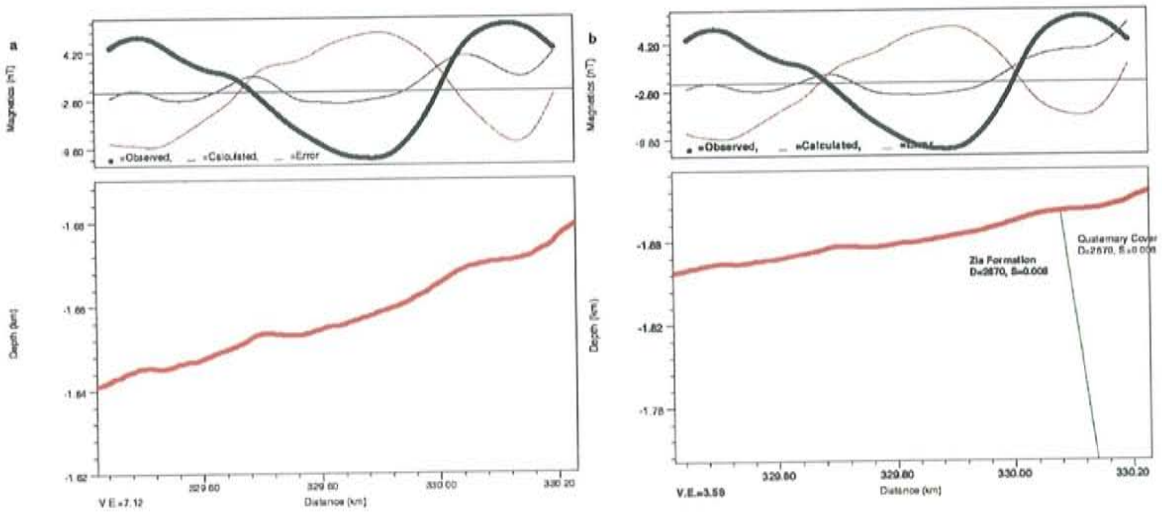

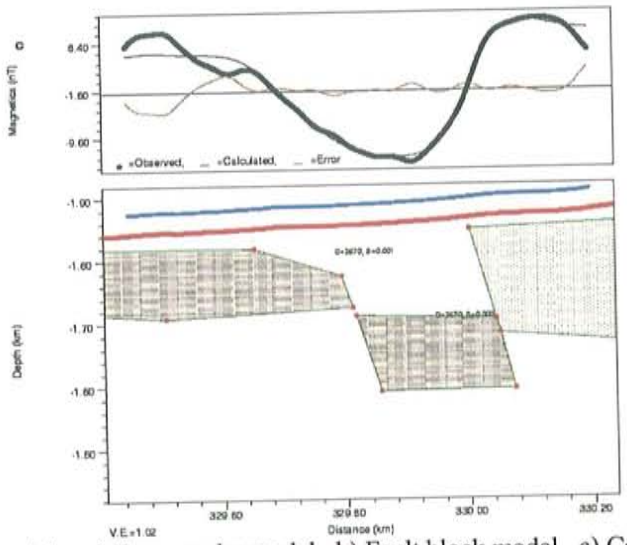

Figure 23. SHF6 data models. a) Topography model. b) Fault block model. c) Complex model to date.

J. SHF7

This line is unique in both its collected signature and complexity displayed in the aeromagnetic data. This area in the aeromagnetic signature included both areas of anomaly offset from mapped fault and anomaly centering along mapped fault. This specific ground line was collected over a centered part of the anomaly. The collected anomaly also exhibits a strong positive peak in the center, as opposed to central troughs. This area also exhibited the most complex topography. For the topographic models, a uniform susceptibility of 0.004 SI was used (Figure 24a). This best showed the variation in topography and kept a close fit to the observed data. There is correlation between topography and anomalous signal. Small troughs off both sides of the main peak appear to have a topographic cause, but the main anomaly still seems poorly modeled. There does appear to be a small-scale feature in the topography that could effect the middle

peak, but even setting to uniform susceptibility of the model to 0.011 SI, it does not appear to be enough topography relief to be causative for the central peak. For the fault model only one fault has been mapped in this area, with a measured dip of approximately 80°. With the fault placed, the apparent correlations of small side troughs are still prevalent, but the central peak is still poorly modeled (Figure 24b). For the lithological model, there are only two lithologic changes along this line. Moving west to east, the first boundary encountered is the mapped fault. It separates a Tertiary sandstone-mudstone complex from a Tertiary conglomerate-sandstone. The second lithologic boundary separates the Tertiary conglomerate-sandstone from Quaternary alluvium fill. The Quaternary sediments are overlain on the conglomerate sandstone in the model. The model shows strong correlation along the eastern edge of the anomaly and similarity along the western edge (Figure 24c). The central peak is still poorly matched in this area though. Further adjustments of inherent susceptibility values within each block strongly skew the model, thus there is deemed to be a feature near the fault causing the strong anomaly.

This data set is unique from the rest, due to its central peak anomaly and the strong correlation of topography with secondary anomalies. A simple thick/thin fault model would not work for this line. The only applicable model for this area would involve some type of anomalous feature contained on or along the hanging wall of this fault, due to the relation of mapped fault and data anomaly. Thus a simple layered model with a strong magnetic feature along that fault plane was required (Figure 24d). Through modeling the apparent best fit was a box like structure buttressed up the side of the fault plane. This structure is approximately 25 to 30 meters wide away from the fault and

approximately 120 to 130 meters of depth within the subsurface. The idea behind this line comes from Smith (personal communications, 2002). Her work covered colluvial wedges along the Sand Hill fault. Through the movement history on a growth fault like the Sand Hill, these colluvial wedges become stacked up on one another through time. These wedges form on the downthrown hanging wall block of a fault, and can be formed by alluvial, eolian, or gravitational processes. The colluvial wedges are thickest closest to the fault; thus in terms of magnetic susceptibility distribution, the colluvial wedges would most likely be a vertical tabular feature of susceptibility buttressed against the fault plane and taper off it's effects on overall susceptibility distribution as it moves away from the fault.

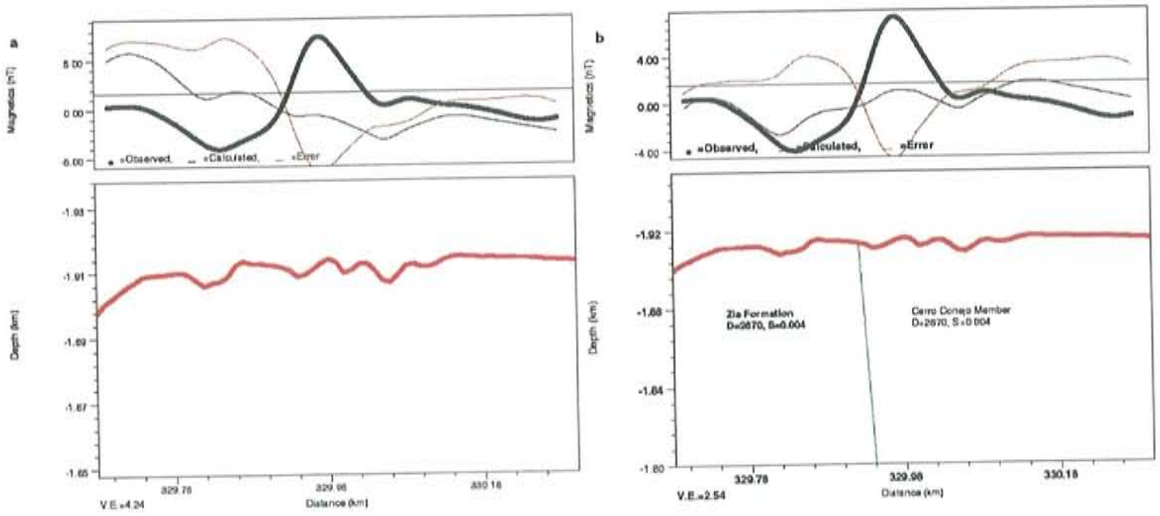

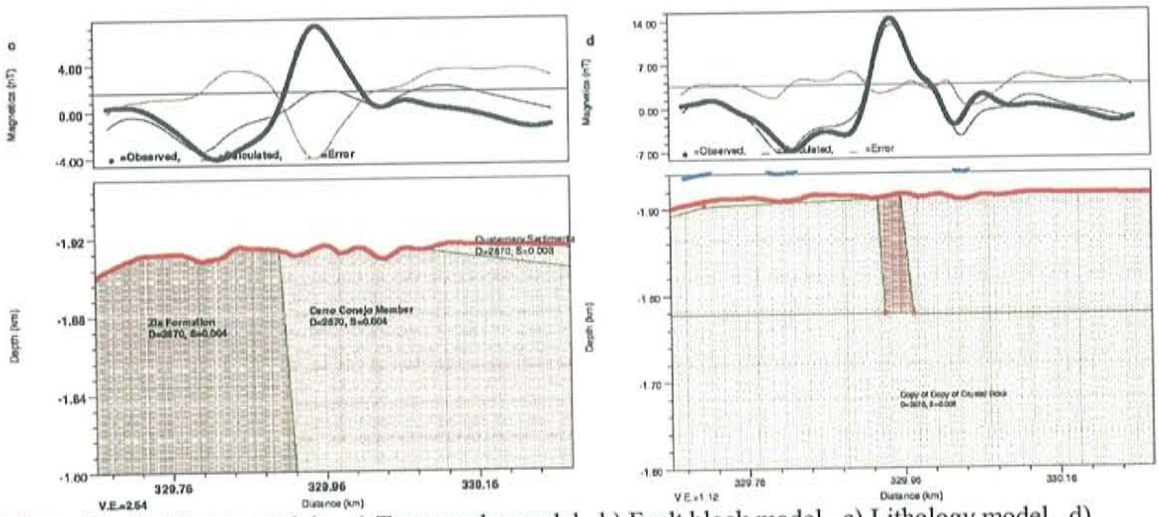

Figure 24. SHF7 data models. a) Topography model. b) Fault block model. c) Lithology model. d) Complex model to date.

This line and its associated model brought up the question of other lines being fit by a similar type model. This model type could be associated with the idea of vertical fluid flow along fault planes (Pierce et al., 1998). Two of the more prominent models, in-terms of strong anomalous peaks, were set up with tabular structures, each had the tabular feature positioned in the best matching spot in the model. Figure 25a shows SHF4 data with two small tabular bodies approximating the two peaks on both sides of the main trough. The fit is not good, especially for the central trough. The topographic peak located approximately center of the data trough produces a peak in the model if there is assumed to be some susceptibility in the overall subsurface. For the actual tabular bodies, the western-most one is fit approximately where the western-most fault has been mapped and appears to match up somewhat with the data. The eastern-most tabular body is more than 100 meters to the east of where the fault has been mapped, and the anomaly produced from it is considerably thinner then the data anomaly. To get the body to approach the width of the data anomaly, it had to be widened to approximately 140 meters wide in the subsurface and have susceptibility close to that of the background

(Figure 25b). SHF2 shows much the same scenario. To place two tabular bodies in a model, the western-most modeled body is approximately 20 meters to the west of the mapped fault. The eastern-most splay is approximately 60 meters to the east of the second mapped fault splay. It also has a peak in the topography that does not match the trough in the data. The correlation is decent on the eastern edge of the line, but poor elsewhere, especially along the anomalous trough in the data (Figure 25c).

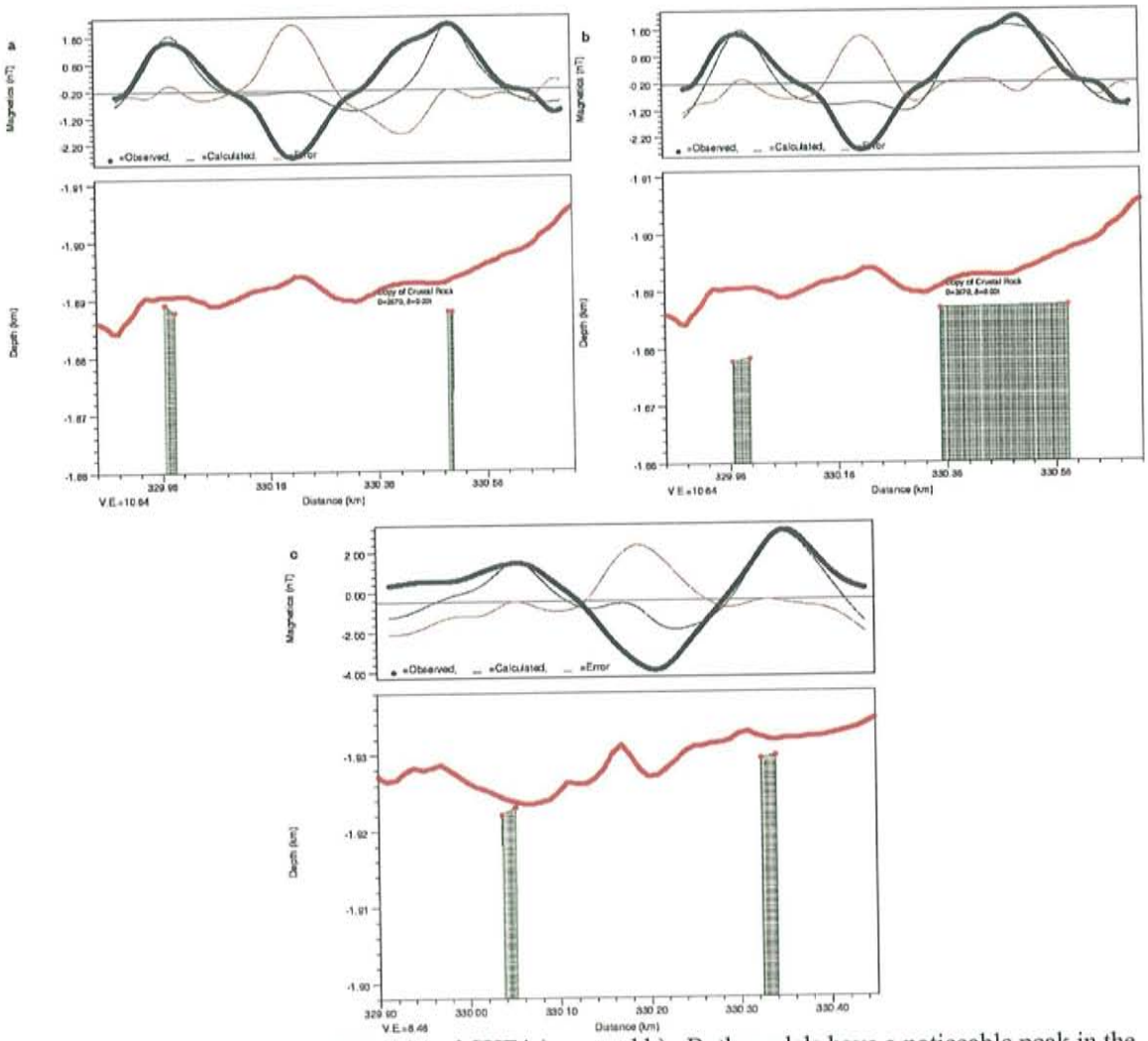

Figure 25. Dyke models for SHF2 (c) and SHF4 (a and b). Both models have a noticeable peak in the topography approximately located under the anomalous troughs in the magnetics data that are counterintuitive to the fitting of the model with data.

K. Line model relations

A comparison of fault mapping via the models as they progress through the various lines is done here (Figure 26). As there was only one fault modeled in SHF1, it easily compares to SHF2. The fault of SHF1 appears in the middle of the two faults modeled in SHF2, but lines up closest with the eastern-most fault in SHF2. The correlation between SHF2 and SHF3 is more complex. The fault from SHF1 does not appear to be there, or has shifted some. The eastern most fault of both SHF2 and SHF3 apparently line up well appearing to be moving eastward as it progresses south, but the second fault modeled in SHF3 seems to have no apparent counterpart in SHF2. This moves into SHF4, which appears to be more similar to SHF2 then SHF3. The main fault of SHF3 does appear to be in SHF4, but slightly shifted. The second fault in SHF3 is present in SHF4, again still progressing eastward. The anomalies from SHF4 and SHF5 appear very similar, but they are in different areas making correlation hard. The eastern-most fault in SHF5 appears to line up with the western-most fault in both SHF3 and SHF4. Thus just comparing the lower three lines, two of the faults present in SHF5 do appear to be the same in SHF6 (Figure 27), but the middle fault in SHF5 does not seem present in SHF6. SHF7 appears separate from the others, both because of the model and its large distance from SHF6, but is it noted that the one fault in SHF7 seems to be modeled in SHF6.

The correlation of mapped faults to model faults also appears to be strong in general, though it is noted these are just visual interpretations and not exact. As the faults are modeled at depth with some dip, there is not a precise determination method. As

well, mapped faults are not completely precise in terms of true GPS position. In general the eastern-most modeled faults in the lines SHF1-SHF4 follow the trend of faulting as has been mapped (Cather et al., 1997). The western-most mapped fault pattern appears to be present as well, but the line of the mapped fault is not clear. In SHF1, the only modeled fault matches up well with the western-most mapped fault. The eastern-most fault in this area does not appear to have any significant contribution to the model. In SHF2, the western-most mapped fault does line up well with a smaller scale fault modeled to the west of the main thick-thin fault. The main modeled fault though has not been mapped in this area. The eastern-most mapped fault does match up somewhat with the high susceptible layer offset up on the eastern edge of SHF2. For SHF3, both modeled faults seemingly match up well with the mapped faults. There is some potential offset on the western-most main fault splay, but that can be attributed to fault dipping angle. SHF4 does not appear to have a match with the main thick-thin fault, but the eastern-most offset fault does match up with the mapped fault in this area. No correlation appears for the western-most mapped fault on this line though. For both SHF5 and SHF6, there does not appear to be any correlation between mapped and modeled faults. As this area was strongly covered in Quaternary sediments, only one fault was mapped in this line. The SHF7 model has a strong dyke-like feature contained within it. This matches up well as a feature located juxtaposed on the hanging wall of the mapped fault.

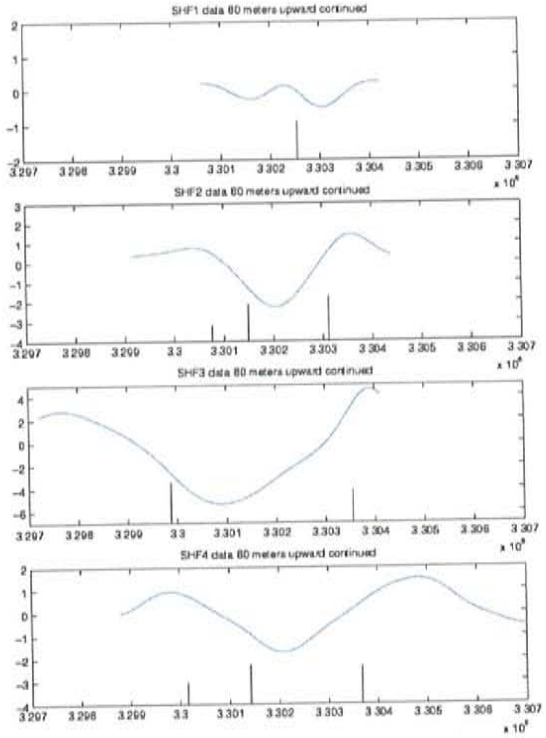

Figure 26. Plot with modeled faults exposures in relation to the magnetics data SHF1-SHF4.

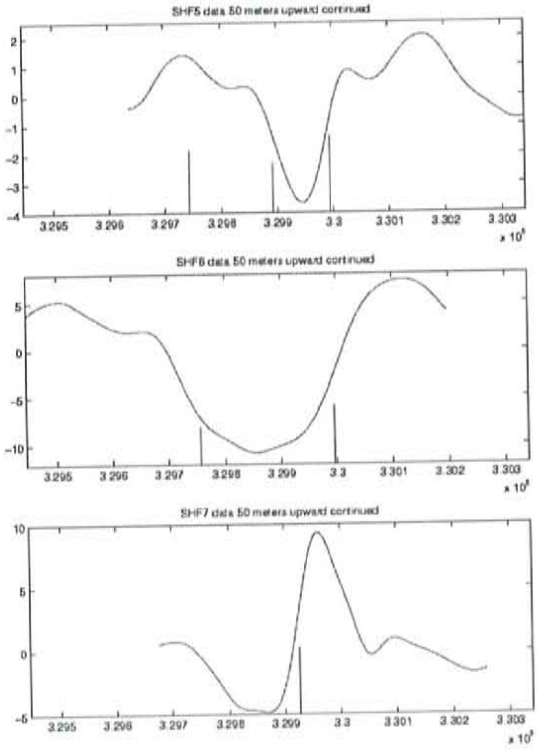

Figure 27. Plot with modeled faults exposures in relation to the magnetics data SHF5-SHF7

Most of the models within this area seemingly fit a thick-thin model within the upper 300 meters of the subsurface as the basic component of modeling. They all appear to be some relationship of the Lower Santa Fe group being offset against itself, with various other middle and upper Santa Fe sediments along the top edges. These models have a seemingly strong correlation with the cross section of Hawley et al. (1995). Additional features within the models appear to be a function of the complex faulting nature within sedimentary basins and the loose sediments contained therein.

VII. Conclusions

The complexity of the Sand Hill fault makes it an excellent fault to perform this type of study on. Through the course of the study, a number of conclusions can be inferred from the data and subsequent models.

First addressing specific questions related to the aeromagnetic data. Areas that exhibited no aeromagnetic signature, but fault was mapped, can be explained by the strength of anomaly relative to the regional trends. The anomalies through the northern parts of the Arroyo de las Cabacillas quadrangle were present, but were relatively smaller then counterpart anomalies more to the south.

For areas within the magnetics data that appeared offset relative to mapped faults, the answer appears to be the fact that there are additional unmapped or buried faults that are the primary source of the anomaly. This conclusion is further enhanced by the fact that the areas in question were mostly covered with Quaternary sediments, thus making fault mapping based on visual investigation a difficult task.

One general conclusion based on the data are also made for this study, is that topography is not the main cause of anomalous magnetic signature. Topography does account for some of the anomaly in certain lines, and almost none of the signature in others. Yet the main anomalous features in the magnetic surveys appear to be completely unrelated to the topography.

All of the data collected appears to best be modeled with blocks located in the upper 300 meters. Thus, shallow structures control the main aspects of the models. Models also require more fault structures then have been mapped in the field. With complex faulting in sedimentary basins, much faulting can go undetected with traditional means of fault mapping and modeling. In some lines, additional complexities required simply adjusting layer thickness and/or shapes. In other lines, the additional complexity required additional faults to be modeled.

In one of the lines that differed from the rest (SHF7), there appears to be a case for strong magnetization located along the hanging wall block of the fault. As the magnetization is not just localized along the fault plane (it is as wide as 100 meters away from the fault plane), the data is felt to represent colluvial wedge stacking in this specific area. Other possibilities are not ruled out, but this idea seems to be most supported by geologic studies.

For the remaining lines, modeling was best fit with juxtaposition of thick-thin magnetic layers against one another. In general, these layers had the same susceptibility with between 50 to 100 meters of offset. These layers would appear to be the same layers that were offset through the faulting process and overfill of sediments onto the hanging wall block (colluvial wedges).

VIII. Appendix A

The following program is a Matlab script writing to perform the upward continuation algorithm for continuation of the magnetics data.

```
clear
clf;
% script to do upward continuation, Dave Wilson, 4/12/02

% input file
inputfile = 'SHF1data.txt';

% output file
outputfile = 'deleteme.txt';

%upward continuation height (negative for up) (same units as input file x)
d=-50;

%number of evenly spaced grid points to interpolate to
npts=1000;

% ---------------------------------------------

Ain = load(inputfile);
A = Ain(:,5:6);
A = [ A Ain(:,1)];
n = length(A(:,1));

    dx = (A(n,1) - A(1,1))/(npts-1);
    dy = (A(n,2) - A(1,2))/(npts-1);
    newx = A(1,1):dx:A(n,1);
    newy = A(1,2):dy:A(n,2);
    newmag = interp1(A(:,1),A(:,3),newx);

 % old upward continuation
    FFmag = fft(newmag);
    FFmag2 = fftshift(FFmag);
    faxis = (-1:2/npts:1-2/npts).*(1/(2*dx));
    filt1 = exp(abs(faxis) .* 2* pi* d);
    FFmag3 = FFmag2 .* filt1;
    mag2 = real(ifft(ifftshift(FFmag3)));

 % remove linear trend
    B = [ newx' ones(size(newx'))];
    B2= B.';
    C=inv(B2*B);
```

```
    D= B.' * newmag';
    m = C * D;
    mline = m(1).*newx + m(2);
    newmag2 = newmag - mline;

% upward continuation
    FFmagpad = fft([ newmag2 zeros(size(newmag2))]);
    FFmag2pad = fftshift(FFmagpad);
    faxis2 = (-1:1/npts:1-1/npts).*(1/(2*dx));
    filt2 = exp(abs(faxis2) .* 2* pi* d);
    FFmag3pad = FFmag2pad .* filt2;
    mag2pad = real(ifft(ifftshift(FFmag3pad)));

% add linear trend back in or leave anomalous signal only
    mag2pad = mag2pad(1:1000);%+mline;

% write output
Dout = [ newx' newy' mag2pad' ];
save(outputfile,'Dout','-ascii')

% plot of true data versus unpadded continuation versus padded continuation
figure(1); clf
    plot(A(:,1),A(:,3))
    hold on
    plot(newx,newmag,'g')
   plot(newx,mag2,'r')
   plot(newx,mag2pad,'k')

% plot of both continuations
figure(2); clf
   plot(newx,mag2pad,'k')
hold on
   plot(newx,mag2,'r')

% plot of padded continuation only
figure(3);
plot(newx,mag2pad,'x');
```

IX. References

Anderson

Burger, H. R., 1992, Exploration Geophysics of the shallow subsurface: Prentice Hall, Englewood Ciffs, NJ.

Cather, S.M., Connell, S.D., Heynekamp, M.R., and Goodwin, L.B., 1997, Geology of the Sky Village SE (Arroyo de Las Calabacillas) 7.5' quadrangle, Sandoval County, New Mexico: New Mexico Bur. Mines and Min. Res. Open-File Digital Geological Map OF-DGM9.

Geometrics, 1995, Geometrics G-858 Magmapper Operations Manual, Geometrics, Inc. Sunnyvale, CA.

Gibson, R.I., and Millegan, P.S., Eds., 1998, Geologic applications of gravity and magnetics: Case histories: Soc. Expl. Geophys. And Am. Assn. Petr. Geol.

Grauch, V.J.S., Hudson, M.R., and Minor, S.A., 2001, Aeromagnetic expression of faults that offset basin fill, Albuquerque basin, New Mexico: Geophysics, 66, p. 707-720.

Grauch, V.J.S., and Millegan, P.S., 1998, Mapping intrabasinal faults from high-resolution aeromagnetic data: The Leading Edge, 17, 53-55.

Hawley, J.W., Haase, C.S., Lozinsky, R.P., 1995, An underground view of the Albuquerque Basin, in, The Water Future of Albuquerque and the Middle Rio Grande Basin, Proceedings of the 39th Annual New Mexico Water Conference, New Mexico Water Resources Research Institute Report 290, p. 37-55.

Heynekamp, M. R., Goodwin, L. B., Mozley, P. S., and Haneberg, W. C., 1999, Controls on fault-zone architecture and fluid flow in poorly lithified sediments, Rio Grande Rift, New Mexico: Implications for fault-zone permeability and fluid flow, in Haneberg, W.C., Mozley, P.S., Moore, K.C., and Goodwin, L.B., eds., Faults and subsurface fluid flow in the shallow crust: Washington, DC, American Geophysical Union, p. 27-49.

Heynekamp, M.R., 1998, Controls on fault-zone architecture and fluid flow in poorly consolidated sediments. The Sand Hill Fault, Central New Mexico: [unpub. Master's dissertation]: Socorro, New Mexico Tech, 73pp.

Hudson, M.R., Mikolas, M., Geissman, J.W., and Allen, B.D., 1999, Paleomagnetic and rock magnetic properties of Santa Fe Group sediments in the 98th Street core hole and correlative surface exposures, Albuquerque Basin, New Mexico: New Mexico Geological Society Guidebook, 50, 355-361.

Lillie, R.J., 1999, Whole Earth Geophysics, Prentice Hall, Upper Saddle River, NJ.

Machette, M.N., 1978, Dating Quaternary faults in the southwestern United States by using buried calcic paleosols: Journal of Research, U.S. Geological Survey, v. 6, p. 369 – 381.

NGA, 2001, GM-SYS User's Guide, Northwest Geophysical Associates, Inc., Corvallis, OR.

Paterson, N.R., and Reeves, C.V., 1985, Application of gravity and magnetic surveys: The state-of-the-art in 1985: Geophysics, 50, 2558-2594.

Pierce, J.W., Goussev, S.A., Charters, R.A., Abercrombie, H.J., and DePaoli, G.R., 1998, Intrasedimentary magnetization by vertical fluid flow and exotic geochemistry: The Leading Edge, 17, 89-92.

Rawling, G.C., 2001, Structural Geology and Hydrogeologic characterization of faults in poorly lithified sediments: [unpub. P.h.D. Dissertation]: Socorro, New Mexico Tech, 210pp.

Redford, M.S., 1980, Magnetic Methods: Geophysics, 45, 1640-1658.

Reynolds, J.M., 1997, An introduction to applied and environmental geophysics: John Wiley & Sons, New York.

Sharma, P.V., 1976, Geophysical methods in geology: Elsevier, New York.

Society of Exploration Geophysicists, 1998, Special section on gravity and magnetics: The Leading Edge, 17, No. 1, 41-119.

Society of Exploration Geophysicists, 2001, Special section on gravity and magnetics: The Leading Edge, 20, No. 8, 863-904.

Talwani, M., and Heirtzler, J.R., 1964, Computation of magnetic anomalies caused by two-dimensional bodies of arbitrary shape, in Parks, G.A., Ed., Computers in the mineral industries, Part 1: Stanford Univ. Publ., Geological Sciences, 9, 464-480.

Won, I.J., and Bevis, M., 1987, Computing the gravitational and magnetic anomalies due to a polygon: Algorithms and Fortran subroutines: Geophysics, 52, 232-238.